Article

Not peer-reviewed version

First *in – Silico* Study of Two *Echinococcus granulosus* Glyceraldehyde-3-Phosphate Dehydrogenase Isoenzymes Recognized by Liver Cystic Echinococcosis Human Sera

Facundo Ariel Agüero , Andrea Maglioco , María Pia Valacco , Alejandra Yaqueline Juárez Valdez , Emilio JA Roldán , Margot Paulino * , Alicia Graciela Fuchs *

Posted Date: 15 September 2025

doi: 10.20944/preprints202509.1185.v1

Keywords: *Echinococcus granulosus*; glyceraldehyde 3 phosphate dehydrogenase; in silico analysis; biomarker; molecular dynamics simulation

 doi:10.20944/preprints202509.1185.v1

Article

First *in –Silico* Study of Two *Echinococcus granulosus* Glyceraldehyde-3-Phosphate Dehydrogenase Isoenzymes Recognized by Liver Cystic Echinococcosis Human Sera

Facundo Ariel Agüero [1,2], Andrea Maglioco [1,2], M. Pía Valacco [2,3], Alejandra Juárez Valdez [2,4], Emilio J.A. Roldán [1], Margot Paulino [5,*] and Alicia G. Fuchs [1,4,*]

[1] Centro de Altos Estudios en Ciencias Humanas y de la Salud, Universidad Abierta Interamericana, Buenos Aires, Argentina
[2] Consejo Nacional de Investigaciones Científicas y Técnicas, Buenos Aires, Argentina
[3] Centro de Estudios Químicos y Biológicos por Espectrometría de Masa, Facultad de Ciencias Exactas y Naturales, Universidad de Buenos Aires, Buenos Aires, Argentina
[4] Instituto Nacional de Parasitología "Dr. Mario Fatala-Chaben", Administración Nacional de Salud "Dr. Carlos Malbrán" Buenos Aires, Argentina
[5] Facultad de Química, Departamento de Experimentación y Teoría de la Materia y sus Aplicaciones, Área Bioinformática, Universidad de la República, Montevideo, República de Uruguay
* Correspondence: margot@fq.edu.uy (M.P.); alicia.fuchs@UAI.edu.ar (A.G.F.)

Abstract

Cystic echinococcosis (CE) is an endemic zoonotic disease caused by *Echinococcus granulosus*, which forms cysts in ungulates' intermediate hosts. Humans are accidental hosts, and CE affects more than one million people worldwide. Imaging remains the diagnostic gold standard, outperforming serological methods. This study presents an *in silico* analysis of two glyceraldehyde-3-phosphate dehydrogenase (GAPDH) isoenzymes from *E. granulosus* (EgGAPDH), isolated from a parasite cell line (EGPE). EgGAPDHs were recognized by sera from CE patients, identified through LC-MS/MS and PCR from metacestodes' cattle liver. One isoenzyme is intracellular (IC) (UniProt: W6UJ19), and the other is extracellular (EC) (UniProt: W6V1T8). GAPDH is involved in host-parasite interactions and metabolic processes. We Characterized the physicochemical properties, linear epitopes, and amino acid domains of EgGAPDH, its hosts and other parasites. W6UJ19 emerged as the most promising isoenzyme as a marker of infection. Molecular dynamics simulations of isoenzymes, performed in the presence or absence of two bisphosphonates (BPs), revealed how drug binding alters conformational epitopes and suggest that enzymatic activity is more likely associated with W6UJ19. Binding affinity analysis using the MMPBSA method revealed that etidronate (EHDP) binds EgGAPDH with greater affinity than phosphate (Pi) and alendronate (AL), in the order: EHDP > Pi > AL.

Keywords: *Echinococcus granulosus*; glyceraldehyde 3 phosphate dehydrogenase; *in silico* analysis; biomarker;-molecular dynamics simulation

1. Introduction

Cystic echinococcosis (CE) is a zoonotic endemic disease produced by the *Echinococcus granulosus* s.s (*E. granulosus*) in the intermediate host. *E. granulosus* s.l. belongs to the class *Cestoda*, and based on the last consensus, it is classified into four genotype clusters: *E. granulosus sensu stricto* (G1-G3), *E. equinus* (G4), *E. ortleppi* (G5) and *E. canadensis* (G6-8/10) [1]. *E. granulosus s.s* (G1/3) is prevalent in both human and livestock populations in Argentina [2]. The World Health Organization (WHO)

 doi:10.20944/preprints202509.1185.v1

classifies CE as a neglected disease. In 2020, it was estimated that one million people were worldwide infected, with an incidence of 50 cases per 100,000 inhabitants in hyperendemic areas. However, prevalence rates reached 5-10% in certain regions of Argentina, Peru, Central Africa and China [3].

The life cycle of the parasite involves an intermediate host, specifically ungulate animals, and accidental hosts such as humans and cats [4]. In the intermediate host, the parasite develops the cystic echinococcosis (CE) characterized by the development of a larval stage unilocular cyst, most commonly located in the liver (65-75 %) and lung (23-30 %) [5] and less frequently in the heart, bone and pelvic organs, and other tissues. The intermediate host is infected by ingesting the oncosphere present on dust, vegetables, dog jaws or fur. The definitive host, a member of the *Canidae* family, becomes infected by ingesting raw, infected viscera, from the intermediate host. Within the intestinal lumen, the embryos develop into hermaphroditic worms that release oncospheres, which are excreted in feces after approximately 5 months of growth and maturation.

Parasitic cysts developed in the intermediate host are composed of two membranes. The outer membrane is acellular, in direct contact with the host's tissues and is composed primarily of glycoproteins and mucins. The inner membrane is a germinal, proliferative layer, where parasite embryos, or protoscoleces (pe), are formed through asexual sprouting. These pe are released into the cyst´s internal cavity, which is filled with hydatid fluid (HF) containing salts, proteins and cells. The presence of the cyst induces a chronic inflammatory response in host tissue, leading to the formation of a poorly vascularized external membrane. In humans, cyst can grow up to five centimeters per year and may disseminate if ruptured due to trauma or other complications.

Cyst evolution in humans is monitored and diagnosed by abdominal ultrasonography, showing characteristic images classified according to the Gharbi classification [6], in active (I, II and III) and inactive (IV and V). Serology is used to support diagnosis, but it is not a reliable tool for CE diagnosis or monitoring patient follow-up due to the occurrence of false-positive and false-negative results, as well as cross-reactions [7]. *E. granulosus* releases factors within the host that interfere with the immune response [8]. The well-characterized antigens used in CE diagnosis are AgB and Ag5. Serological methods, such as, ELISA and Western blot, are performed using a homogenate of *ex vivo* larval tissues or HF collected from infected ungulate animals at slaughterhouses. However, the use of recombinant *E. granulosus* major antigen, rAgB, has not significantly improved the diagnostic performance of serological tests compared to native antigens [9,10].

Our group is working on the identification of new antigens from *E. granulosus* s.l. The antigenic profile of EGPE cell line, derived from bovine *E. granulosus* G1 pe [11], demonstrated greater sensitivity in detecting serum reactivity from patients compared to HF obtained from sheep infected with *E. granulosus* G1 [12]. EGPE cells were grown in liquid medium and biphasic agarose medium, forming cystic colonies [11]. This cellular model enables the study of proteins primarily in intracellular (IC) and extracellular (EC) compartments. Using immune-identification, by CE patient sera, and LC-MS/MS methodologies, we identified four histones eluted by immune affinity from different subcellular localizations, IC and EC compartments [13].

In this work, we studied two out of five glyceraldehyde-3-phosphate dehydrogenase (GAPDH) isoenzymes described in *E. granulosus* recognized by CE patient sera and identified by LC-MS/MS methodology. One was found in the IC and the other in the EC compartment. GAPDH is a homotetrameric enzyme of the glycolytic pathway composed of four subunits of 36 kDa. Each subunit contains an active center with the coenzyme NAD+ and the substrate-binding regions responsible for reducing NAD+ to NADH, necessary for the function of the electron transport chain and the conversion of the glyceraldehyde-3-phosphate into 1,3-bisphosphoglycerate, later metabolized in the glycolytic pathway to produce ATP. GAPDH is known as a "housekeeping" gene and is localized in the cytoplasm of all animals' somatic cells at high concentrations, accounting for approximately 5 to 15% of total soluble protein [14]. In cestodes, this enzyme has been colocalized with tegmental calcareous corpuscles, as observed in *Taenia solium* metacestodes [15] Additionally, other roles have been attributed to GAPDH, such as vesicle and exosome biogenesis [16,17] and the binding to lactoferrin, ferritin [18], mucins [19] and fibronectin [20].GAPDH is sensitive to free oxygen radicals,

 doi:10.20944/preprints202509.1185.v1

which trigger its dissociation and its later migration to the nucleus, contributing to cell death and apoptosis [21]. In *Trichomonas vaginalis*, iron availability has been shown to regulate both the synthesis and surface localization of the enzyme [22]. Moreover, multiple GAPDH isoenzymes and isoforms have also been described in various species with different organelle associations, subcellular localization, and different roles. The impact of GAPDH on parasite-host relations is probably contributing to the parasite adhesion and development, considering its presence in vesicles and exosomes secreted by the parasite [17].

Bisphosphonates (BP) are synthetic analogs of bisphosphoric acid, in which the central oxygen atom is replaced by a carbon atom. These compounds exhibit pleiotropic mechanisms of action. Antiparasitic activity of BP has been proposed in *Apicomplexa*, primarily through the inhibition of farnesyl diphosphate synthase [23], interference with acidocalcisomes by mimicking the hydroxyapatite surface [24,25], and inhibition of mitochondrial ubiquinone [26]. In *Trypanosoma bruceii* BP have been shown to inhibit solenyl biphosphate synthase [27]. As a biological effect, BP reduce the size of *Toxoplasma gondii* cysts in the central nervous system [28,29]. Furthermore, amino-BP have been reported to inhibit the synthesis of glyceraldehyde-3- phosphate dehydrogenase in cancer cell lines [30]. The antiparasitic effects of BP depend on both the specific compound used and the biological characteristics of the parasite.

Our research group has studied the effects of five BP, commonly used in humans and veterinary medicine, on EGPE cell line). We observed the inhibition of cell growth and cystic colony development upon treatment with ibandronate, etidronate (EHDP) and olpadronate. These effects were accompanied by decreases in intracellular ATP and free calcium levels [31,32]. The chemical structure of BP determines their molecular targets. Non-amino BP, which constitute the first compound generation (e.g., EHDP), act by forming insoluble complexes with ATP. In contrast, amino-BP, such as AL, inhibit the mevalonate pathways, affecting growth factor signaling and cellular metabolism [33]. The pleiotropic actions of BP are attributed to their chemical simplicity.

To date, no bibliographic references have been found that provide a detailed molecular characterization of EgGAPDH beyond its genetic sequences. However, studies have reported inhibitory effects of praziquantel and albendazole on capsular GAPDH in *E. granulosus* metacestodes [34]. Additionally, growth inhibition of metacestodes by antibodies against recombinant *Echinococcus multilocularis* GAPDH [35] highlights the relevance of studying this enzyme in *Echinococcus* spp.

GAPDH is one of the most representative constitutive cellular proteins, known for its multiple biological functions. In this study, two isoenzymes of EgGAPDH were investigated, one predominantly IC and the other EC. Both isoenzymes were recognized by sera from CE patients and identified by LC-MS/MS. The corresponding genes were amplified by PCR from *ex vivo E. granulosus* s.s. (G1 genotype) metacestode. The physicochemical properties and amino acid sequence differences of identified EgGAPDH isoenzymes were analyzed and compared with GAPDH sequences from other described *E.granulosus'* GAPDH, other parasites and host organisms.

For the first time, *in silico* tridimensional models of both EgGAPDH isoenzymes were constructed. Linear and conformational B-cell epitopes were predicted and mapped onto the modeled structures. These models were subsequently subjected to molecular dynamics simulations to assess their stability and were used to study interactions with two BP commonly used in human and veterinary medicine: EHDP and AL. Previous *in vitro* studies indicated that EHDP inhibited parasite cell growth, whereas AL did not. The molecular interactions between BP and EgGAPDH may influence enzyme activity and alter the exposure of epitopes on the protein surface.

The results contribute to a better understanding of the structure, physicochemical properties, and immunological features of EgGAPDH isoenzymes. Moreover, this study offers insights into the probable differences in enzymatic activity and interaction with BP, which may explain the variable efficacy of BP in inhibiting parasite cell growth *in vitro* and their potential application in antiparasitic therapy.

2. Results

 doi:10.20944/preprints202509.1185.v1

2.1. Characterization of EgGAPDH

2.1.1. Genomic Sequences Identification

EGPE cell proteins and supernatant proteins from EGPE colonies were recognized by antibodies from CE human sera but not by sera from patients with fasciolasis or cysticercosis. Two GAPDH isoenzymes were identified by LC-MS/MS: one present in the cell homogenate (IC; UniProt W6UJ19) and another in the colony supernatant (EC; UniProt W6V1T8). DNA sequences of both GADPDH isoenzymes were obtained from *E. granulosus* ss/ G1 metacestode isolated from cow liver. The nucleotide identity between the two isoenzymes was 74.11%. PCR results are shown in Figure 1a,b.

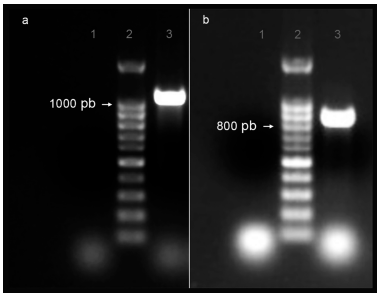

Figure 1. PCR products of EgGAPDH isoenzymes DNA were extracted from *ex vivo* liver cattle metacestode *E.granulosus* G1/ s.s. a) Amplification of isoenzyme W6UJ19; b) amplification of isoenzyme W6V1T8. Lane 1: negative control; lane 2: Base pair marker (bp) and lane 3: PCR product.

The obtained product sequences were analyzed using BLAST against published *E. granulosus* sequences. For isoenzyme W6UJ19, the forward sequence showed 86.74% identity with 99% coverage relative to the NCBI Reference Sequence XM_024492989.1. The reverse sequence displayed 93.53% identity with 78% coverage. In the case of isoenzyme W6V1T8, the forward sequence exhibited 81.31% identity and 72. % coverage compared to the NCBI Reference Sequence XM_024494574.1. The reverse sequence showed 98.54% identity with 83% coverage. (Figure S1a–d).

2.1.2. Amino Acid Sequence's Identity

Amino acid sequence identity with other *E. granulosus* GAPDH isoenzymes, none of which were recognized by human serum in reactivity assays, was evaluated. Isoenzymes W6UPZ5 and A0A068WMZ6 (UniProt) showed 26.42% and 28.63% identity, respectively, with W6UJ19 and 25.87% and 27.53% identity with W6V1T8. In contrast, isoenzyme A0A058WSX5 showed 99.70% identity with W6UJ19 and 73.13% identity with W6V1T8. Isoenzymes A0A068WKQ2 (UniProt) and A0A096ZQK3 (UniProt) exhibited 71.64% and 73.12% identity with the IC isoenzyme (W6UJ19), and 96.13% and 99.79% identity with the EC isoenzyme (W6V1T8).

The amino acid sequences of the EgGAPDH isoenzymes W6UJ19 and W6V1T8 were compared with GAPDH sequences from other species. W6UJ19 showed the following sequence identities: *E. multilocularis* 71.73%, *T. solium* 75.6%, *Fasciola hepatica* 73.94%, *L. mexicana* 53.43%, *H. sapiens* (UniProt P04406) 53.43%, *Bos taurus* 70.57% and *Ovis aries* 70.81%. In contrast, W6V1T8 shared higher sequence identities with most of these species: *E. multilocularis* 97%, *T. solium* 91.96%, *F. hepatica* 81.91%, *H. sapiens* 70.78%, *B. taurus* 75.38 % and *O. aries* 75.78%. *The exception was L. mexicana*, with which W6V1T8 shared a lower identity (51.80%) compared to W6UJ19.

 doi:10.20944/preprints202509.1185.v1

2.1.3. Physicochemical Characterization

All GAPDH isoenzymes analyzed were predicted to be thermostable and lack a classical signal peptide for secretion. The predictive half-lives for W6UJ19, W6V1T8 and *L. mexicana* GAPDH were similar, with an estimated 30 hours *in vitro* in mammalian reticulocytes, over 20 hours in yeast and more than 10 hours in *Escherichia coli*, according to ProtParam analysis. Despite these similarities, notable differences were observed in the predicted physicochemical properties between the *E. granulosus* isoenzymes, W6V1T8 exhibited a higher net positive charge, greater hydrophobicity and a higher isoelectric point compared to W6UJ19 (Table 1).

Table 1. Comparative GAPDH physicochemical properties from different species.

GAPDH Specie (UniProt)	M.W / amino acid number	Charge	Isoelectric point	Protein instability	Aliphatic index	Gravy index
***Echinococcus granulosus* (W6UJ19)**	338 / 36.6	+1 (R + K 37; N + E: 36)	7.56	24.45	86.55	-0.100
***Echinococcus granulosus* (W6V1T8)**	336 / 36.1	+3 (R+ L 35; N + E: 32)	8.44	21.82	85.89	0,004
***Echinococcus multilocularis* (Q27652)**	336 / 36.39	+7 (R+K: 39; N+E: 32)	9.02	27.10	84.40	-0.090
***Taenia solium* (A8R8Q4)**	336 / 36.26	+3 (R+K: 35; N+E: 32)	8.44	19.73	86.19	-0.029
***Fasciola hepatica* (A0A068LJN3)**	338 / 36.93	0 (R+K: 37; N+E: 37)	7.1	25.15	84.76	-0.109
***Leishmania mexicana* (Q27890)**	361 / 39.03	+7 (R+K: 42; N+ E:35)	9.05	27.63	83.96	-0.115
***Homo sapiens* (P04406)**	335 / 36.049	+3 (R+K: 36; N+E: 33)	8.57	15.04	85.55	-0.112
***Bos taurus* (P10096)**	333 / 35.87	+3 (R+K: 36; N+ E:33)	8.51	17.7	84.89	-0.078
***Ovis aries* (Q28554)**	322 / 34.73	+1 (R+K: 34; N+E: 33)	7.83	17.38	85.09	-0.091

2.2. EgGAPDH Secondary and Tertiary Structure Stability

2.2.1. Secondary Structure

The secondary structures of both EgGAPDH were found to be highly similar. For W6UJ19 and W6V1T8, the predicted structures were as follows: α-helix, 33.80% and 33.93%; extended strand, 23.67% and 24.70%; β-turn, 9.17% and 8.33 % and random coil, 31.36% and 33.04%, respectively (Figure 2a,b).

 doi:10.20944/preprints202509.1185.v1

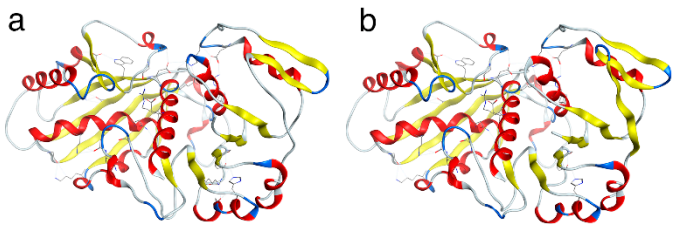

Figure 2. EgGAPDH secondary structure. Obtained by MOE shows one subunit of each EgGAPDH a) It shows W6UJ19, an intracellular isoenzyme and in b) the W6V1T8, the extracellular one. Structural elements are indicated, the α-helix in red; the β-turn in blue; the extended strand in yellow and the random coil in grey.

2.2.2. Tertiary Structure of EgGAPDH Isoenzymes Stability

The subunit of each isoenzyme was assayed for the molecular structure stability. The root mean square deviation (RMSD) between the ab initio models generated with Phyre2 and the AlpHafold3 models was 1.27 Å for W6UJ19 and 1.42 Å for W6V1T8. After 100 ns of molecular dynamics simulation, the tertiary structures remained within a stable conformational range, consistent with structural stability throughout the simulation (Figure 3a,b).

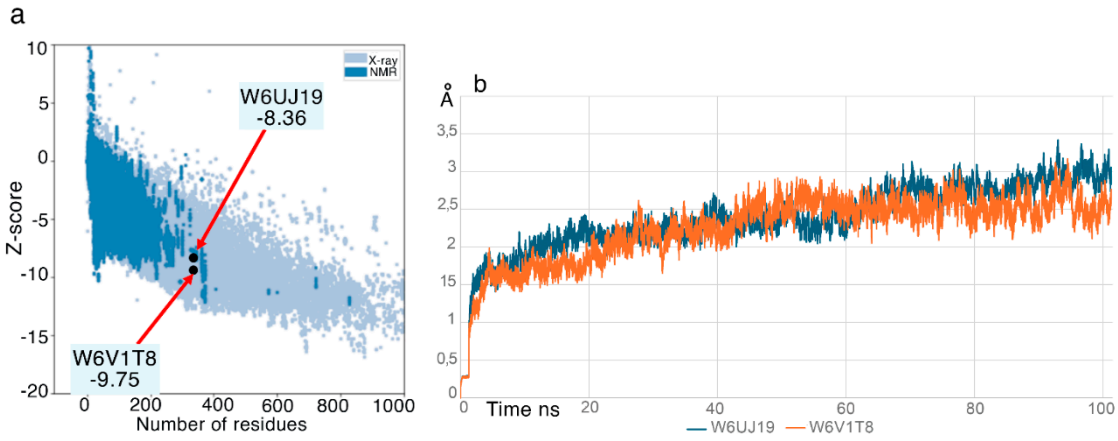

Figure 3. Tertiary structure stability of EgGAPDH monomers. In a) Model quality assessment of Phyre2 models using PROSA-web. Z scores are shown in blue for NMR structures and light blue for X-ray structures. In b) Structural stability over 100 ns of molecular dynamics production simulation was evaluated by RMSD.

2.2.3. Isoenzymes Quaternary Structures and Linear Epitopes

Monomers of both isoenzymes were assembled in a quaternary structure through non-covalent bonds (Figure 4a,b).

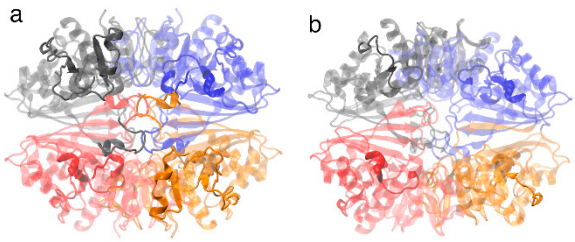

Figure 4. Quaternary structure and linear epitope mapping of glyceraldehyde-3-phosphate dehydrogenase isoenzymes. In a) it shows intracellular isoenzyme W6UJ19 and in b) extracellular isoenzyme W6V1T8. The quaternary structures are shown as homotetramers. The four subunits are shown in colors. Linear epitopes are highlighted in opaque.

 doi:10.20944/preprints202509.1185.v1

The sequences of the predicted EgLEP(s) were compared with the amino acid sequences of GAPDH from other species including *E. multilocularis*, *T. solium*, *F. hepatica*, *L. mexicana*, *H. sapiens*, *B. taurus* and *O. aries*. No similarities were found with the intracellular isoenzyme of GAPDH. However, the extracellular isoenzyme W6V1T8 showed similarity with *T. solium* (UniProt A8R8Q4) in the linear epitope region K138-T153, and with *E. multilocularis* (UniProt Q27652) in regions K138-T153 and F286-I301.

- Post-translational linear epitope modifications.

The complete enzyme is formed by the assembly of four identical subunits without covalent bonds. Linear epitopes (LEP) were predicted for both W6UJ19 and W6V1T8. Table 2 shows the amino acid sequences of the linear epitopes along with their associated predicted post-translational modifications.

Table 2. Glyceraldehyde-3-phosphate dehydrogenase linear epitopes (LEP) and the post –translational modifications.

GAPDH Isoenzyme	LEP	Residue	Predicted modification(s)
W6UJ19	A82-EAIPWDKDGVYYVV-E97	W87	Nitration
		K89	Ubiquitination
	D88-KDGVYYVVESTGVN-T103	K89	Ubiquitination
	S123-APSKDAPTFVVGVN-L138	-	-
	K140-YDPSMTIVSNASCT-T155	S149	Phosphorylation
		N150	Glycosylation
		S152	Phosphorylation
		T154	Phosphorylation
	Q186-KLVDGPNPKGWRDG-R201	K195	Acetylation Methylation
	D282-VVSMDFRTSTASST-F297	S285	Phosphorylation
	F288-RTSTASSTFDANAG-I303	-	-
W6V1T8	K138-YDPSMKVVSNASCT-T153	S147	Phosphorylation
		N148	Glycosylation
		C151	Nitrosylation
		S150	Phosphorylation
		T152	Phosphorylation
		T153	Phosphorylation
	F286-LSTTCSSTFDARAG-I301	-	-

2.3. Isoenzymes Docking and Molecular Dynamics Simulation

2.3.1. Isoenzymes Docking

GAPDH is composed of four identical subunits, each containing an active site for substrate binding (glyceraldehyde 3-phosphate), as well as binding sites for NAD+ and inorganic phosphate (Pi) (Figure 5). These functional sites were conserved among the GAPDH proteins analyzed in this study. However, *L. mexicana* and *O. aries* showed greater variability in the conformational binding sites for NAD+ and Pi (Table S1).

 doi:10.20944/preprints202509.1185.v1

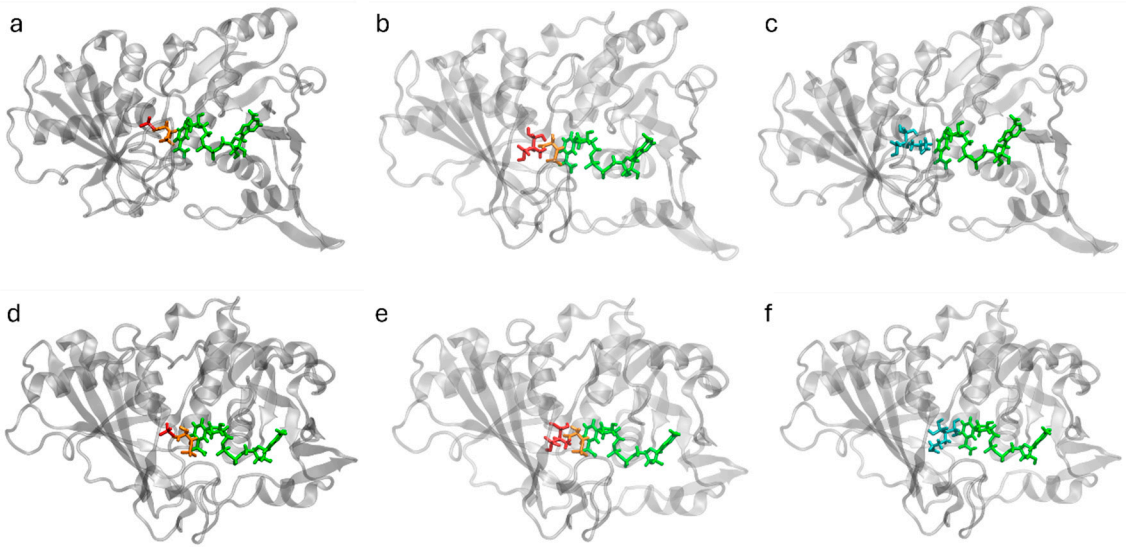

Figure 5. GAPDH and ligands docked in subunit A. Up: GAPDH W6UJ19 (intracellular) from left to the right: a) Protein with G3P (orange), Pi (red) and NAD+ (green), b) G3P (orange), EHDP (red) and NAD+ (green), c) ALE (cyan) and NAD+ (green). Down: GAPDH W6V1T8 (extracellular) from left to the right: d) Protein with G3P (orange), Pi (red) and NAD+ (green), e) G3P (orange), EHDP (red) and NAD+ (green), f) AL (cyan) and NAD+ (green).

- Isoenzymes potential energy with interactions

The potential energy of the quaternary structure, including interactions with the substrate, Pi and NAD+ is summarized in Table 3. Although the Van der Waals energy was positive, the total energy was negative. Both electrostatic and the Van der Waals energy values remained stable throughout the 100-ns molecular dynamics simulation performed using NAMD2. Overall, the potential energy profiles of both isoenzymes were shown in Figure S2.

Table 3. Total Potential energy of both GAPDH isoenzymes during molecular dynamics simulation after equilibration step (100 ns of unrestrained production), partitioned into electrostatic and Van der Waals contribution, all values are in kcal/mol.

GAPDH		Electrostatic		Van der Waals		Total Potential Energy	
		Mean	SD	Mean	SD	Mean	SD
W6UJ19	MD	-498905.11	484.6043	35705.02	302.8204	-433534.22	357.6353
W6V1T8	MD	-500354.14	483.1283	35967.32	303.1194	-435622.22	344.5178

2.3.2. EgGAPDH's Amino Acids Binding Substrate, Pi and NAD+ During Dynamics Simulation

Throughout the molecular dynamics simulations, each subunit of EgGAPDH showed two binding sites corresponding to the substrate, Pi and NAD+. These two sites corresponded to the beginning or the end of the 100 ns simulation. While the binding sites involved similar amino acids overall, there were differences between isoenzymes and among subunits. The amino acids involved in substrate, Pi and NAD+ binding for the intracellular isoform are shown in Figure 6a, and for the extracellular isoenzyme in Figure 6b. (More interaction details in 2D ligand interaction plot were shown in Figures S3 and S4)

 doi:10.20944/preprints202509.1185.v1

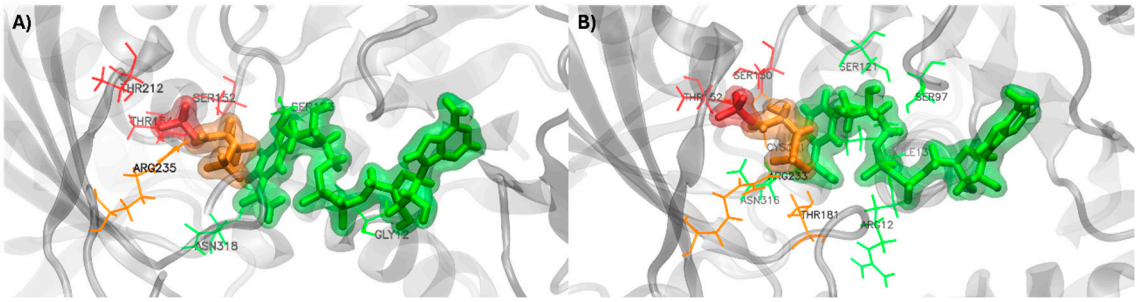

Figure 6. Ligand interactions of Pi (red), G3P (orange) and NAD+ in subunit A of EgGAPDH a) intracellular W6UJ19 and b) extracellular W6V1T8. Residues are highlighted in sticks, in the same color as the ligands they interact with.

- Substrate binding

The residue R233 or R235 was involved in substrate binding of the monomers A, B and C in the IC and monomers A and B of the EC isoenzyme at the beginning of the simulation. At the end of the simulation, this binding was maintained in monomers A and B in the IC, and appeared in all the monomers (A, B, C and D) of the EC isoenzyme.

- Inorganic phosphorus binding

For Pi binding, R233 is involved at the end of the simulation in monomers A, B and C of the IC isoenzyme. In contrast, for the EC isoenzyme, R233 was involved in Pi interaction only in subunit C, with no Pi binding observed in the other monomers at the end of the simulation.

- NAD^+ binding

NAD+ binding interactions presented greater variability between subunits at the initial time point than at the end of the simulation, particularly in subunit A of the IC isoenzyme. Subunit C of the EC isoenzyme displayed different NAD+ interacting residues between the start and the end of the simulation, while subunit D did not interact with NAD+ at the end of the simulation.

2.3.3. The Binding Free Energy (ΔG) for Substrate, Pi and NAD^+

The binding free energy (ΔG) values were calculated using the MMPBSA method based on the last 100 frames of the simulation. The binding free energy varied among the subunits of each GAPDH isoenzyme in which it is noticeable that amino acidic interaction pattern may vary between subunits (Table S1). The binding of the substrate to monomer A yielded a ΔG binding: -10.6968, ± IC95% 1.005 for W6UJ19 and -4.72 ± CI 95% 0.64 for W6V1T8. In contrast, NAD+ binding resulted in negative ΔG values only in monomers B (-4.0176, CI 95% ± 0.725) and D (-0.61, CI 95% ± 0.55) of W6V1T8. The calculated ΔG values for Pi were positive across all subunits and isoenzymes.

2.4. Interaction of BP with both GAPDH Isoenzymes

Two BP, AL and EHDP were docked *in silico*, showing stable molecular interactions with both GAPDH isoenzymes. These interactions did not alter the interaction potential energy, showing the same to those showed in Table 3 and Figure S2. The structural stability of both enzymes in the presence of each BP is shown in Figure 7a,b, through RMSD profiles.

 doi:10.20944/preprints202509.1185.v1

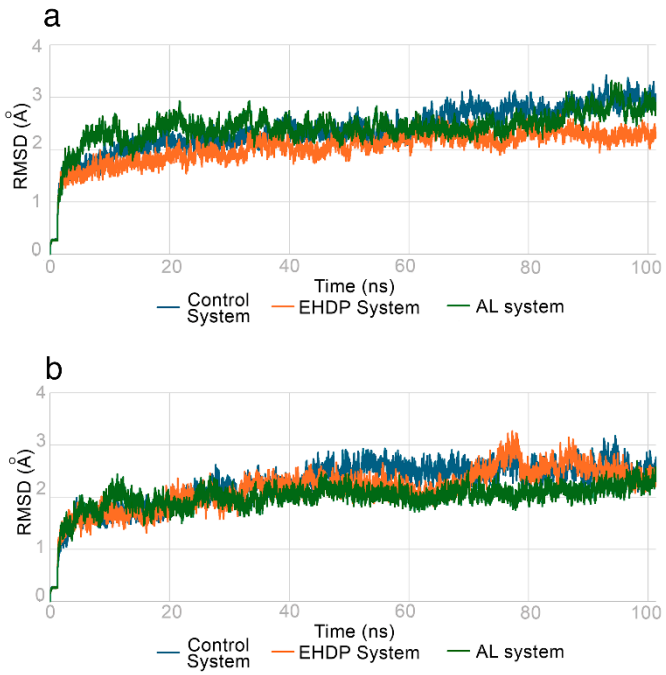

Figure 7. RMSD values of **EgGAPDH** with the addition of BP. Root mean square deviation (RMSD) profiles over 100 ns of molecular dynamics simulation showing the structural stability of W6UJ19 (a) and W6V1T8 (b). The control system is the enzyme with substrate, Pi and NAD^+ without BP. EHDP system is the isoenzyme with EHDP, substrate and NAD^+ and AL system is isoenzyme with AL and NAD^+.

Despite similar structural stability, differences were observed in the interactions between the two BP and EgGAPDH. AL did not support co-binding of the substrate and Pi, while EHDP was able to dock with G3P at the active site, although it did not support Pi interaction.

2.4.1. Docking Affinity

- EHDP increased Pi docking

After docking the EHDP in the presence of NAD+, Pi, and G3P, establishing an interaction zone (docking site) consisting of a sphere at 4.5A centered on G3P, we observed that the EHDP was positioned superimposed on the Pi, so a new situation was modelled in which the EHDP is positioned in the same place as the Pi, having displaced the Pi.

Using the 'placement none' resource, which allows the static interaction situation to be measured in each case, the interaction energy of the Pi in the NAD+, Pi, G3P complex without the EHDP present was measured (Table 4):

Table 4. ΔG of binding estimated for Pi and EHDP to EgGAPDH intracellular and extracellular in each simulation system.

Ligand	ΔG of binding (kcal/mol)	
	GAPDH W6UJ19	GAPDH W6V1T8
Pi (system GAPHD Pi, G3P, NAD+)	-2.136 ± 1.366	-3.477 ± 0.098
EHDP (system GAPHD EHDP, G3P, NAD+)	-4.413 ± 0.313	-4.363 ± 0.331

All measured averages were submitted to a student's "t" Test resulting $p < 0.05$ confirming that the differences are significant.

- AL increased NAD^+ docking

After docking with AL in both enzymes, containing G3P, Pi, and NAD+, it was observed that AL was positioned in the same area as G3P and Pi. Therefore, a putative model was generated of an enzyme that is blocked by AL, having displaced itself during the interaction of all components to G3P

 doi:10.20944/preprints202509.1185.v1

and Pi. This does not mean that the docking has caused such displacement. It is only proposing a possible model that could explain the interaction of AL with NAD+.

In these putative models, AL showed different influences on the binding of NAD+ at the site in both EgGAPDH isoenzymes (Table 5).

Table 5. ΔG of binding estimated for NAD+ to EgGAPDH intracellular and extracellular in control and AL simulation system.

Ligand	ΔG of binding (kcal/mol)	
	GAPDH W6UJ19	GAPDH W6V1T8
NAD+ (system GAPHD Pi, G3P, NAD+)	-7.727 ± 0.674	– 9.274± 0.419
NAD+ (system GAPHD AL, NAD+)	-9.418 ± 0.644	-10.376 ± 0.771

In consequence, the substitution of AL by G3P and Pi, resulted in an energy interaction significantly increased for the NAD+ molecule (student "t" test $p < 0.05$).

2.4.2. BP Effect on the Isoenzyme Substrate Affinity Studied by Molecular Dynamics.

A measurement of the free energy differences (ΔG) of ligands and enzymes was made by MMPBSA method. The Table 6 shows that the addition of BP changed the subunit affinity for the substrate, NAD+ and PI, accordingly with EHDP or AL

Table 6. Binding free energy (ΔG, kcal/mol) estimated by MMPBSA method for EgGAPDH isoenzymes in the presence and absence of BP.

MMPBSA of EgGAPDH with and without BP							
CONTROL		W6UJ19			W6V1T8		
Subunit	Ligands	Mean	± sd	± CI 95%	Mean	± sd	± CI 95%
A	G3P	-10.6968	5.1229	1.005	-4,724	3,2619	0,64
B		15.4506	5.1449	1.01	3,9659	4,4619	0,875
C		16.4556	4.8065	0.945	44,9831	7,6067	1,49
D		24.028	3.8583	0.755	6,2637	4,5538	0,895
A	NAD^+	22.4688	6.7112	1.315	6,6577	5,4992	1,08
B		32.8592	7.3992	1.45	-4,0176	3,6996	0,725
C		13.5946	4.3631	0.855	23,7809	5,5271	1,08
D		6.0962	4.2739	0.835	-0,61	2,8136	0,55
A	Pi	29.6458	6.7445	1.325	6,7074	3	0,59
B		39.1984	7.6647	1.5	1,2245	10,312	2,025
C		22.235	6.1243	1.205	45,3445	5,9314	1,165
D		37.2889	7.0652	1.385	2,1399	10,741	2,11
EHDP							
A	G3P	-16.9965	4.7622	0.935	-7,9112	3,9841	0,78
B		5.2706	3.8102	0.75	-7,5877	3,8438	0,755
C		-5.1953	7.1869	1.405	-7,9317	3,1745	0,62
D		-9.1029	5.5589	1.09	-14,587	4,1819	0,82
A	NAD^+	2.4725	10.0795	1.975	1,7223	5,9318	1,16
B		7.3854	4.7754	0.935	6,221	5,0763	0,995
C		27.6537	8.7531	1.715	-4,6031	3,9027	0,765
D		28.9197	5.1906	1.02	4,4928	4,5107	0,885
A	EHDP	-6.6067	3.3539	0.655	-4,0724	3,0422	0,595
B		-7.1715	2.9301	0.575	0,5011	3,9765	0,78
C		0.815	5.1088	1.005	-11,8148	3,0683	0,605
D		2.0767	4.4194	0.865	-1,3616	3,2844	1,29
AL							

 doi:10.20944/preprints202509.1185.v1

A	NAD+	24.1947	7.3184	1.435	9.1407	6.0582	1.19
B		2.1941	4.4401	0.87	8.8646	5.4337	1.065
C		-3.7258	3.5832	0.705	5.2785	4.2828	0.84
D		-3.0283	2.003	0.39	-3.2583	3.9806	0.78
A	AL	19.1598	3.9525	0.77	7.624	3.2452	0.635
B		-1.2968	2.2008	0.43	0.3786	2.3406	0.46
C		4.3972	3.5114	0.685	6.9541	3.3836	0.665
D		8.2511	4.1911	0.82	-1.8823	13.8439	2.715

- Substrate affinity.

Upon EHDP addition, substrate binding affinity became evident in both isoenzymes. Conversely, AL inhibited G3P binding to the active site, showing only weak binding in subunit B of W6UJ19 and subunit D of W6V1T8. Both GAPDH isoenzymes exhibited a variable and, in some cases, weak or no affinity for the substrate depending on the studied subunit (G3P) (Table 6). This instantaneous measurement makes evident the diversity among subunits with respect to their binding.

- Pi affinity

The Pi interaction may be very transient with both isoenzymes, and its binding could not be reliably detected under control conditions. However, EHDP was able to bind to the Pi site of both isoenzymes but in W6V1T8 it occurred though with lower affinity. In contrast, AL exhibited weak binding to the Pi conformational site on W6UJ19 and on W6V1T8 (Table 6).

- NAD+ affinity

No NAD+ binding was detected in W6UJ19, either with or without EHDP. In W6V1T8, NAD+ binding was observed and with EHDP addition detectable NAD+ binding was observed in another subunit. AL, however, promoted NAD+ binding in W6UJ19, specifically in subunits C and D, and in W6V1T8 in subunit D, although with weaker value than in the control subunit B (Table 6).

2.4.3. Amino Acids Involved in BP Interactions

In tables 7 and 8 all amino acids interacting with all ligands are informed.

Table 7. List of Amino acid interacting with ligands in the EgGAPDH intracellular in each simulation system. In bold: amino acid that makes frequent contacts with ligands.

W6UJ19	Initial			Final		
Control	G3P	Pi	NAD+	G3P	Pi	NAD+
Subunit A	**R235**(2)	T154 S152 T212	G12 (2) N318(2) **S123**(2)	**R235**(3) His180(2) T183 C153	K195(3) R235(2)	**S123**
Subunit B	C153 **H180** **T183**	C153(2) T154 H180	G12 **R13** **D35** N318(2)	R235(2) **H180 (2)** **T183**	R235(3) K195(2)	**R13** **D35** D190
Subunit C	R235(2)	T154	R13 H180 EA319 **K187**	T212(2) G213	R235(2) H180(2)	E319(2) D190 N193 **K187**
Subunit D	H180	T154(2) H180 G213	**D35** S98 C153	C153	K195 R235	**D35** T99
W6UJ19		Initial			Final	

 doi:10.20944/preprints202509.1185.v1

EHDP	G3P	EHDP	NAD	G3P	EHDP	NAD
Subunit A	R235(2)	T154(2) Q211 T212 G213 **R235**	G12(2) S98 S123(2) N318(2)	T183 H180(3)	Q211 **R235**	D337
Subunit B	**C153** H180 T183	C153 T154 H180	G12 R13 D35 N318(2)	**C153**	D199(2) Q211(2) P209	K195
Subunit C	R235(2)	T154(2) **T212**	R13 H180 K187 **E319**	H180(2)	**T212**	P192 **E319**
Subunit D	**C153**	T154 **Q211** **T212**(2) G213	**D35** S98 C153	S123 **C153**(2) H180(2) T183 N318	**Q211** **T212** R235	**D35** E319
W6UJ19	Initial			Final		
AL	AL	NAD		AL	NAD	
Subunit A	T154(2) Q211 T212(2) G213 R235	G12(2) S98 S123(2) N318(2)		S123	A184 E319 K187 D190	
Subunit B	C153 T154 H180	G12 R13 D35 N318(2)		I38	-	
Subunit C	T212 T154(2)	R13 H180 **K187** E319		S126 D128(2) A217	T103(2) I122 **K187**	
Subunit D	T154 Q211 T212(2) G213	D35 S98 C153		A124 S149 S152	-	

Table 8. List of Amino acid interacting with ligands in the EgGAPDH extracellular in each simulation system. In bold: amino acid that makes frequent contacts with ligands.

W6V1T8	Initial			Final		
Control	G3P	Pi	NAD	G3P	Pi	NAD
Subunit A	T181 C151 **R233(2)**	S150 C151(2) T152(2)	**R12** I13 S97 **S121(2)** N316(2)	**R233(3)** K193(2)	-	**R12(2)** D34(2) T98 **S121** E317
Subunit B	C151 **R233**	C151 T152(2)	R12(2) **D34(2)** S121 N316(2)	**R233(2)** K193(2)	-	G11 **D34(2)**

 doi:10.20944/preprints202509.1185.v1

Subunit C	C151	S150 C151(2) T152 T210	R12 I13 S97(2) Y320	R233	R233(2) K233(3)	T181 A182 P237
Subunit D	Cys151(2)	S150 C151 T152(2)	G11(2) R12 I13	N101 K193 R233(3)	-	-
W6V1T8	Initial			Final		
EHDP	G3P	EHDP	NAD	G3P	EHDP	NAD
Subunit A	C151 T181 **R233**	T152(2) T210	G11 **R12** I13 S121(2) N316(2)	K193(2) **R233(2)**	-	F10 **R12** D34(2) F36
Subunit B	S150 C151 **R233**	T152(2)	**R12**(2) **D34** E78 **S121** N316(2) E317	K193(2) **R233(2)**	-	F10 **R12** **D34**(2) **S121**
Subunit C	C151	C151(2) T152 H178	**R12** I13 P35 E78 S97(2) Y320	K193(2)	G99	G11 **R12** D34(2)
Subunit D	C151 T183	C151 **T152**	G11 R12 I13 P123(2)	K193 R233(2)	**T152** T210	P35 S97 T98 S121 **P123** T181 T183 K192
W6V1T8	Initial			Final		
AL	AL		NAD	AL		NAD
Subunit A	C151		G11 R12 I13 S121(2) D316(2)	T181		F10 D34(2) F36
Subunit B	C151		**R12** **I13** **D34** E78 C151 E317	D165 N166		G11 **R12**(2) **I13** **D34**(2)
Subunit C	C151(2) E317		**R12** I13 S97(2) Y320	N316		**R12** D34(2) E317
Subunit D	C151(2) H178		G11(2) R12	-		P190 K185

 doi:10.20944/preprints202509.1185.v1

	I13 D34	K192

- EHDP interacts with W6UJ19

In Figure 8 the main interactions with the EgGAPDH W6UJ19 are shown. Figure S5 shows a 2D ligand interaction plot between EHDP and WUUJ19.

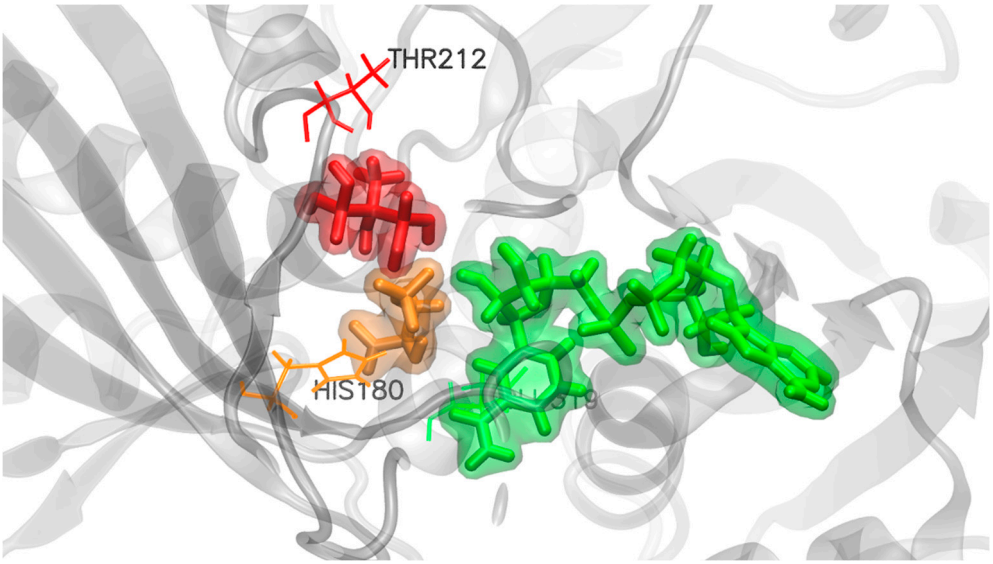

Figure 8. Ligand interaction of G3P (orange), EHDP (red) and NAD+ (green) with EgGAPDH W6UJ19 at the end of simulation (100ns). Residues are highlighted in sticks in the same color as the ligand they interact with.

- Amino acid interaction in W6V1T8 with EHDP

In Figure 9 the main interactions with the EgGAPDH W6V1T8 are shown. Figure S6 a 2D ligand interaction plot between EHDP and W6V1T8 is shown.

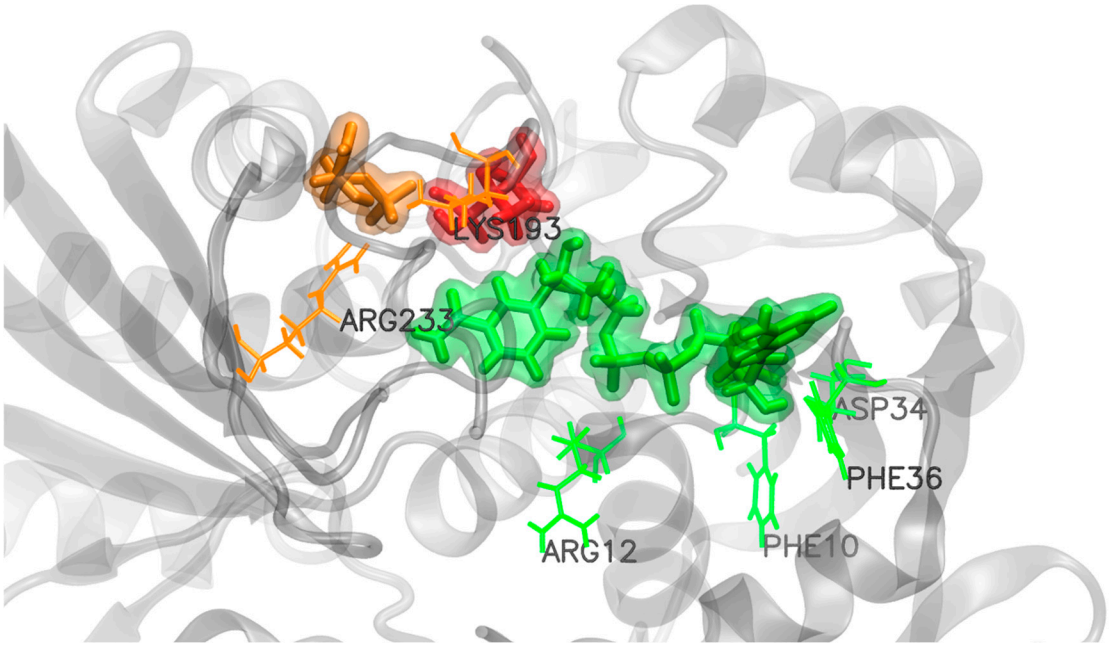

Figure 9. Ligand interaction of G3P (orange), EHDP (red) and NAD+ (green) with EgGAPDH W6V1T8 at the end of simulation. Residues are highlighted in sticks in the same color as the ligand they interact with.

- Amino acid interaction of W6UJ19 and W6V1T8 with AL

 doi:10.20944/preprints202509.1185.v1

In Figures 10 and 11 the main interactions of AL with the EgGAPDH W6UJ19 and W6V1T8 are shown. In Figures S7 and S8, the 2D ligand interaction plots are shown.

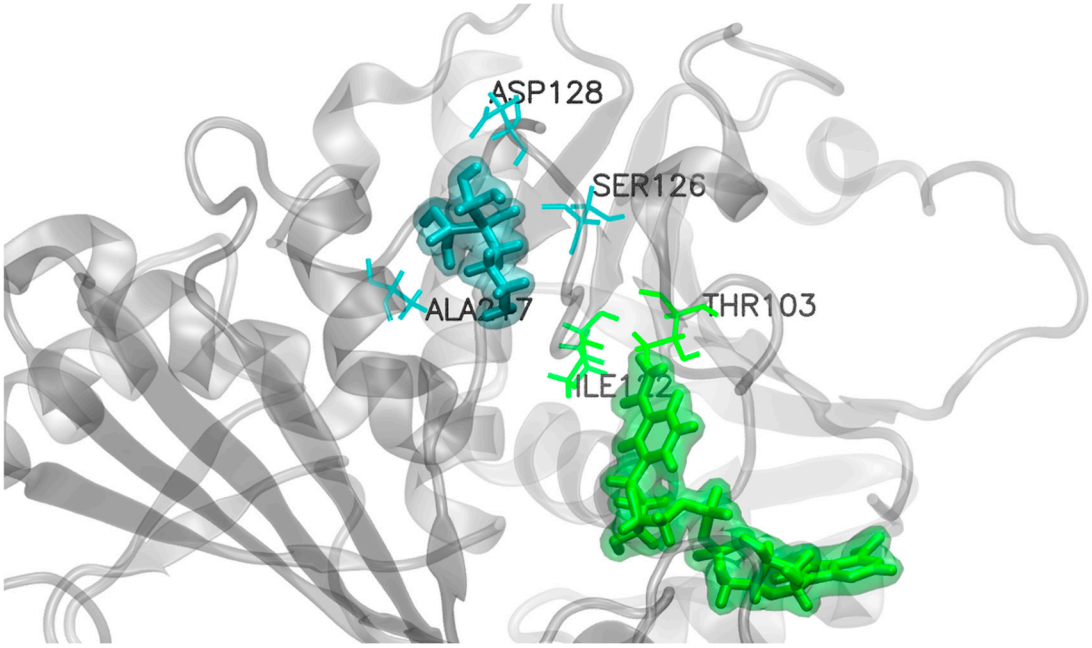

Figure 10. Ligand interaction of AL (cyan) and NAD+ (green) with EgGAPDH W6UJ19 at the end of simulation. Residues are highlighted in sticks with the same color of the ligand they are interacting with.

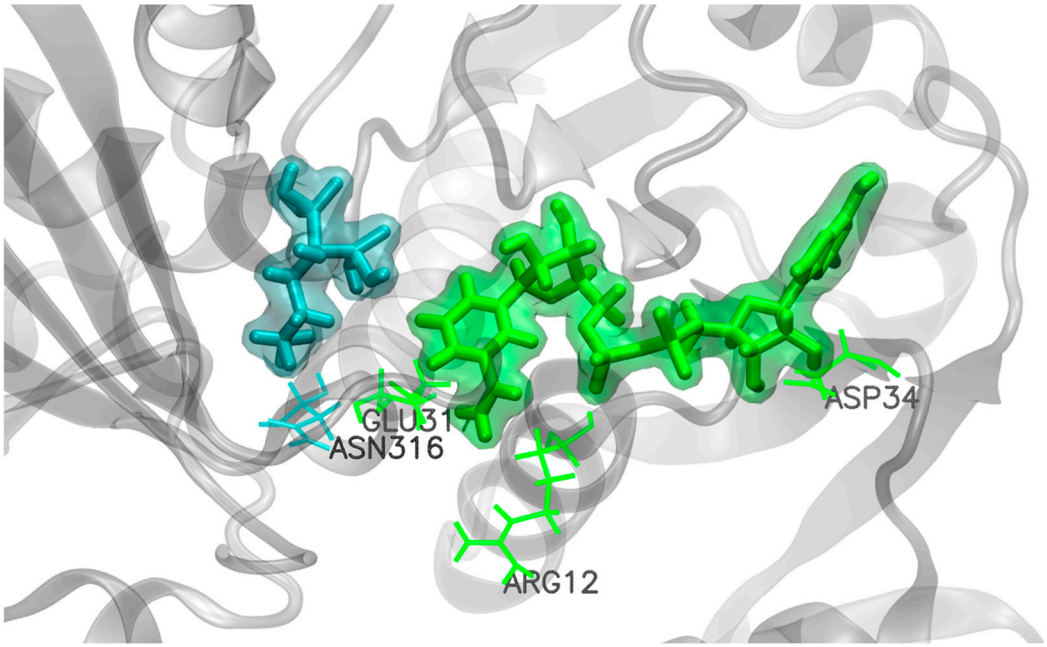

Figure 11. Ligand interaction of AL (cyan) and NAD+ (green) with EgGAPDH W6V1T8 at the end of simulation. Residues are highlighted in sticks with the same color of the ligand they interact with.

2.4. Conformational Epitopes and its Modification by the BP Interactions

2.4.1. Conformational Epitopes

Surface conformational epitopes were identified in both isoenzymes (Figure 12a,b)

 doi:10.20944/preprints202509.1185.v1

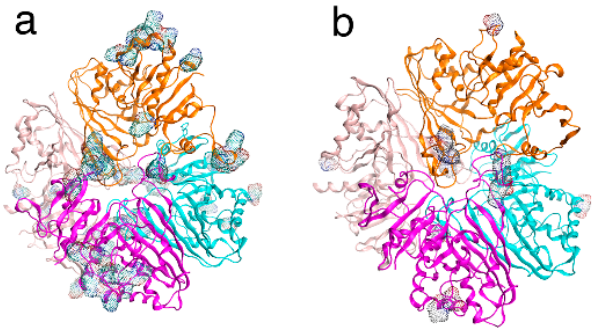

Figure 12. Conformational epitopes of GAPDH isoenzymes. Homotetramers are illustrated with conformational epitopes mapped onto the molecular surface as dots colored according to atomic elements. Chain A is shown in orange, chain B in purple, chain C in cyan, and chain D in gray. (a) Intracellular W6UJ19 and (b) extracellular isoenzyme W6V1T8.

The intracellular isoenzyme (UniProt W6UJ19) exhibited a greater number of conformational antigenic sites than the extracellular isoenzyme (UniProt W6V1T8). Subunit A was the most antigenic in the intracellular isoenzyme, while subunit B was the most antigenic in the extracellular isoenzyme, based on the number of amino acid residues exposed in conformational epitopes (Table 9).

Although. BP established non-covalent interactions with amino acid residues, they altered the surface exposure of the conformational epitopes. The effect of BP on the number and composition of amino acids in the conformational epitopes was most evident with EHDP on W6UJ19. The interaction of BP with conformational epitopes of both isoenzymes is summarized in Table 9.

Table 9. Conformational epitopes, post-translational modifications and changes induced by BP on EgGAPDH W6UJ19 intracellular and W6V1T8 extracellular isoenzymes. System simulations: 1-Control: Pi, G3P and NAD+. 2-EHDP: EHDP, G3P and NAD+. 3-AL: AL and NAD+. Post-translational modifications:–CH_3: methylation, -CH_3CO: acetylation, Ph: phosphorylation and Ubiq: ubiquitination.

Isoenzyme	System	Chain A	Chain B	Chain C	Chain D
W6UJ19	Control	K63, D64, G65, K66, L80, K89, A106, K107, G109, A110, L112, K113, N114, N115, S144, N193, P194, K195	L80, N81, E83, A108, G109, A110, H111, L112, K113, N114, N115, S144, N193, P194	E79, L80, N81, A82, E83, K89, K113, S144, T185, N193, P194, K195, G200, D337	I38, D39, D64, N81, A82, A106, G109, K113, S144, P192, N193, P194
	AL	D64, G65, K66, L80, N81, K89, A106, K107, G109, A110, L112, K113, N114, N115, S144, P192, N193, P194, K195	L80, N81, A82, A84, I85, P86, W87, D88, K89, D90, A108, G109, A110, H111, L112, K113, N114, S144, N193, P194, K195	L80, N81, A82, E83, K89, H111, S144, P192, N193, P194, K195, G200	N81, A106, A110, K113, N114, N115, S144, T185, N193, P194, K195
	EHDP	D39, K63, D64, G65, K66, K107, G109, A110, K113, N114, N115, S144, N193, P194, K195, G196, D337	T41, L112, K113, S144, P192, N193, P194, K195	L80, N81, A82, E83, A106, S144, N193, P194, K195	N81, K107, A110, H111, K113, N114, N115, S144, P194, K195, G196, G200
Post-translational modifications	-CH_3/-CH_3CO	K66 and K195	K195	K195	K195
	Ubiq	K89	K89	K89	-
	Ph	-	-	-	T185

 doi:10.20944/preprints202509.1185.v1

W6V1T8	Control	S142, K192, K193	P141, S142, K192, K193	K192, D335	S142, K192
	AL	P141, S142, K192	S142, K192	S142	P141, K193
	EHDP	K192	S142, K192	D38, K138, K192, K193	P190, K192
Post-translational modifications	-CH_3	K192	K192	K192	K192
	-CH_3/-CH_3CO	K193	K193	K193	K193

3. Discussion

GAPDH is a housekeeping protein, highly represented in cells with regulated enzymatic activity whose transcription and intracellular localization are regulated by feeding or cell proliferation [36]. GAPDH is a highly conserved protein throughout evolution, functioning in the glycolysis pathway by catalyzing the conversion of D-glyceraldehyde 3-phosphate, NAD^+, and (Pi) into 1,3-bisphosphoglycerate and NADH, thereby connecting glycolysis with the respiratory chain. The enzymatic activity depends on the integrity of its quaternary structure, sustained by NAD+ interaction and the absence of negative cooperativity among its monomers, as demonstrated in studies on yeast GAPDH [37]. However, several additional functions have been attributed to GAPDH in cellular biology, including roles in endocytosis [38], fusion of plasma [39] and nuclear membranes [40] and autophagy [41]. Furthermore, partially oxidized GAPDH acylphosphatase activity, which may contribute to glycolysis by coupling with oxidative phosphorylation [42]. Depending on its subcellular localization, GAPDH can perform distinct functions. Nuclear GAPDH, whose localization is cell-cycle dependent, is proposed to play a protective role against DNA damage at telomeres caused by ceramide and toxins [43].

In addition, GAPDH contributes to cellular adaptability and defense against pathogens by participating in protein biogenesis and the regulation of gene expression [44]. Extracellular GAPDH has also been implicated in host-parasite interaction; for example, during leishmaniasis infection, it has been shown to downregulate TNF-α expression in host cells [45].

Given its multiple roles and physiological functions, GAPDH has been proposed as a pharmacological target in cancer, neurological diseases and chronic parasitic infections [46]. Despite its high evolutionary conservation, GAPDH can elicit an immune response. Recombinant *E. multilocularis* GAPDH has been tested in laboratory animals to prevent metacestode development [47].

Our group is searching for novel antigenic proteins to serve as serological markers for the diagnosis and monitoring of CE, while also exploring BP targets on *E. granulosus* proteins. Using immunoaffinity purification with sera from CE patients and protein extracts from the EGPE cell line, we identified *E. granulosus* proteins by LC-MS/MS. We prioritized protein families detected in both the cell homogenate and the cell colony supernatant. Histones were the first group of proteins studied [13], and in this work, we present the results of our investigation on EgGAPDH isoenzymes, following the same conceptual approach.

This is the first work presenting the *in silico* model of two GAPDH isoenzymes from *E. granulosus* ss/G1, recognized by sera from CE patients with liver cysts. These isoenzymes were found in different subcellular localizations, W6UJ19 (UniProt) in IC and W6V1T8 (UniProt) in EC. Analyzing metacestode vesicles by LC-MS/MS method, with different metabolic activity was found correlation between W6V1T8 abundance (emPAI) and vesicle metabolic activity instead, W6UJ19 showed consistent relative abundance regardless of metabolic activity [48]. Physicochemical differences between the two isoenzymes were observed, particularly in their isoelectric points and net molecular charges, both of which were higher in the EC isoenzyme. Both isoenzymes were detected by PCR in ex vivo metacestode samples. The genetic identity between IC and EC isoenzymes was approximately 74%. In contrast, other EgGAPDH isoenzymes not recognized by immunosera (UniProt W6UPZ5 or A0A068WMZ6) shared only ~ 20% identity with the IC and EC isoenzymes. The IC isoenzyme (UniProt W6UJ19) emerged as the main candidate for differential diagnosis,

 doi:10.20944/preprints202509.1185.v1

showing approximately 53% sequence identity with the human GAPDH and approximately 70% identity with GAPDH sequences from E. *multilocularis*, *T. solium* and *F. hepatica*, as well as 55% identity with *L. mexicana*. The IC isoenzyme (UniProt W6UJ19) is also the most promising candidate for constructing a recombinant multiepitope antigen. Notably, it does not share predicted linear epitopes with *E. multilocularis* or *T. solium* in the regions spanning residues S123-L138 and F288-I303. Additionally, no post-translational modifications were predicted in these epitope-containing sequences. Moreover, an antibody reactivity rate between W6V1T8 and W6UJ19 could be useful to determine infection prognosis and treatment success [48].

Molecular dynamics simulations showed that the IC isoenzyme presented a greater affinity for both the substrate and Pi, maintaining more stable amino acid interactions throughout the simulation compared to the EC isoenzyme. Although enzymatic activity assays were not performed, the simulation results suggest that the IC isoform has a higher probability of exhibiting enzymatic activity in the *E. granulosus* metacestode. In contrast, the EC isoform, likely localized in secretion vesicles and /or calcareous corpuscles, appears to participate primarily in host-parasite interaction [15], potentially through protein-protein interactions that facilitate parasite attachment. According to our findings, the quaternary structure of the enzyme remained intact even when the conformational sites for NAD+ or Pi binding were lost by the end of the molecular dynamics simulations. While the quaternary structure of the enzyme is essential for enzymatic activity, it is likely also required for the protein´s non-enzymatic functions, particularly those related to intercellular or intracellular interactions. GAPDH lacks a classical secretion signal peptide, suggesting that its ability to be secreted may depend on interactions with carrier proteins that facilitate its translocation to other cellular compartments [49,50].

Among the BP studied, EHDP reduced cell growth, whereas AL did not produce any measurable effect on *in vitro* cell behavior, beyond a reduction in ATP levels. This BP acts via different mechanisms: EHDP leads to the accumulation of non-degradable ATP analogs [51], while AL inhibits the protein prenylation pathway. EHDP showed stronger binding to both GAPDH isoenzymes than Pi, although pyrophosphate (PPi) exhibited the highest binding affinity ($p< 0.005$ concerning EHDP, data not shown). However, PPi was unable to substitute Pi in the catalytic activity of GAPDH [52]. Unlike PPi, EHDP is not degraded by pyrophosphatases. EHDP also enhanced substrate binding to the IC enzyme and modified the conformational sites for substrate, Pi and NAD+ binding throughout the molecular dynamics simulation, from initiation to completion, suggesting a potential increase in enzymatic activity. Consequently, we can assume that the GAPDH model with EHDP and without Pi has increased affinity for the substrate in both isoenzymes.

In contrast, AL exhibited lower affinity for GAPDH compared to both the substrate and Pi. EHDP bound more strongly than Pi and previous studies have reported that phosphonates can interact with GAPDH by binding after Pi removal; the acyl-enzyme intermediate is expected to enhance activity [53]. However, an increase in GAPDH activity may also lead to elevated production of reactive oxygen species, which could overwhelm the cell´s antioxidant defenses and modify the enzyme´s active site, affecting its ability to bind substrate or Pi [54].

One of the known metabolic effects of EHDP is the reduction of glycolysis rate and the promotion of glycogen storage [55], without altering intracellular Pi concentration or uptake [56]. In previous experiments, we observed a decrease in EGPE cell growth after 72 H of EHDP treatment. This selective effect on parasite cells could be attributed to the limited antioxidant capacity of *E. granulosus*, as neither superoxide dismutase nor the thioredoxin system was overexpressed in response to H_2O_2 challenge [57]. In fact, EHDP is the BP with less effect on bone metabolism at used dose in humans and animals [51,58,59].

Since BPs modify conformational sites involved in ligand binding, we investigated further whether BP binding could also alter the conformational epitopes of GAPDH. Indeed, our results showed that BP binding affected conformational epitopes, either increasing or decreasing the number of amino acids involved in these antigenic regions.

 doi:10.20944/preprints202509.1185.v1

Several studies have explored the immunological effects of BP, demonstrating their potential as adjuvant therapies [60] and their ability to promote prolonged antigen persistence within immune cells. However, these studies often did not distinguish whether the immunological modulation was due to BP interference in mevalonate pathway or a direct effect on the antigenic molecule itself [61].

4. Materials and Methods

4.1. Ethics Statement and Serum Samples

Serum samples from CE patients were obtained by Dr. Jorge Gentile at the Hospital Municipal Ramón Santamarina, Tandil, Argentina. Dr. Elizabeth Luz Sánchez Romaní, from the' Laboratorio de Zoonosis Parasitaria CNSP-INS, Peru,' provided sera samples from patients with cysticercosis and fascioliasis. The Ethics Committee of the 'Universidad Abierta Interamericana, Buenos Aires, Argentina', approved all protocols and procedures (number 01011) [12].

4.2. Characterization of EgGAPDH

4.2.1. EGPE Cell Culture, Protein Extracts, and Supernatant

EGPE is a cell line derived from bovine *E. granulosus* pe G1, maintained in our laboratory. Cells used in the experiments corresponded to passages 35 to 40. EGPE cells were cultured, as previously described [11]., in medium 199 (Sigma), 1 mM sodium pyruvate (sodium salt, extra pure, Anhedra, Beijing, China) and 78 µg/mL β-mercaptoethanol (Merck, Darmstadt, Germany) at pH 7.9 (37°C; CO2:air; 5/95%). EGPE cell colonies were performed in 2% agarose (20,000 cells/well) [11]. After 20 days of cell growth in a liquid medium, the protein extracts were obtained. EGPE cells were washed five times with DPBS and incubated in lysis buffer (8 mmol/L CHAPS, MP Biomedicals, 10 mmol/L Tris –HCl, pH 8, 2 mmol/L EDTA, 0.1% B-mercaptoethanol, MP Biomedicals, and 1/100 protease inhibitor cocktail, Sigma-Aldrich), at 4°C for 2 hours. The samples were then frozen-thawed three times and spun down at 10,000 x g. [12].

Cell colonies were grown for 5 days without medium change, supernatants were obtained, and cell debris was removed by centrifuging the supernatants three times (3,000 rpm). Finally, samples were aliquoted and stored at -20°C until use.

4.2.2. Protein Identification

The methodology was previously described by Maglioco et al., 2022 [13]. Briefly, protein fractions were obtained by separating cell extracts based on molecular weight using a Sephacryl S200 HR column (GE Healthcare). Eluted protein fractions were identified by absorbance (205-280 nm) using a spectrophotometer (Biowave II+, Biochrome Ltd., Cambridge, England). Each protein fraction and EGPE supernatant were concentrated through a 3 kDa cut-off membrane concentrator (Pierce, Thermo Scientific). Antigenic protein fractions and EGPE supernatant were analyzed by Western blot using a pool of sera from 11 patients with hepatic CE. Reactive protein fractions were subsequently purified by affinity chromatography using Protein G HP SpinTrap columns (GE Healthcare). Sera from patients with cysticercosis and fascioliasis were used as controls. Eluted proteins were concentrated through a 3 kDa cut-off membrane concentrator (Pierce, Thermo Scientific).

A 15% SDS–PAGE was performed to concentrate and clean up the protein extracts before in-gel digestion. Protein bands were visualized by Coomassie blue staining, excised, destained, washed, reduced, alkylated and then digested in-gel with 100 ng Trypsin (Promega V5111). The resulting peptides were recovered by elution and analyzed by nano LC-MS/MS, at the Proteomics Core Facility of the CEQUIBIEM, Faculty of Exact Sciences, University of Buenos Aires/IQUIBICEN CONICET. Protein identification was performed using the *E. granulosus* database from UniProt.org [62], following the procedure described by Maglioco et al., 2022 [13].

 doi:10.20944/preprints202509.1185.v1

4.2.3. EgGAPDH genomic sequence

E. granulosus DNA was extracted from a G1 genotype metacestode isolated from the liver of a cow obtained at a local slaughterhouse in Buenos Aires, Argentina (provided by Dr. Tatiana Aronowicz, SENASA). Primers for amplification of the complete GAPDH gene sequence were designed using the Primer-Blast tool available on the NCBI website [63]. The fragment size ranged from ≈800 -1,000bp.

For W6UJ19 (IC), the forward primer was GAGGCCCAACACCGGAATTA and the reverse CCACGGGTTTCAGTAATGAGC (Tm 54.36 °C; extension time: 1min 3 sec). For W6V1T8 (EC), the forward primer was TCGAGAAGGCCTCGGTAAGA and the reverse primer was TCCAGCGGGAGCCTTAATGA (Tm 54 °C; extension time: 50 sec.). Primers were purchased from Gene Biotech SRL, Buenos Aires, Argentina. Each reaction tube contained: 1.5 mM MgCl2 (5x, Colorless GoTaq® Reaction Buffer, Promega, Madison, WI, USA), 0.2 mM of dNTPs mix (dGTP, dCTP, dTTP and dATP, Promega, Madison, WI, USA), 1 µM forward primer, 1 µM reverse primer, 1.25 units of DNA polymerase (GoTaq® polymerase, Promega, Madison, WI, USA), 18 ng of DNA template and nuclease-free water up to 25 µL (ultrapure, PB-L, Productos Bio-lógicos). DNA amplification was performed with an initial denaturation step at 95° C for 2 min, followed by 35 cycles of denaturation at 95° C for 1 min, primer annealing at the respective temperature for each primer pair for 1 min, and extension at 72° C for a time determined by the expected product size. A final extension step was carried out at 72° C for 5 min. Reactions were conducted using a Mastercycler gradient thermocycler (Eppendorf, Hamburg, Germany). Then, 17.5 µL of each product was analyzed by agarose gel electrophoresis (LE molecular biology grade, PB-L, Productos Bio-Lógicos, Buenos Aires, Argentina) using a 100-1,100-bp ladder (Dongsheng Biotech Co., Ltd., Guangzhou, China) as a size marker. DNA bands were excised and purified using the Wizard® SV Gel and PCR Clean Up System (Promega Co., USA). Purified PCR products were sequenced at the CEDIE "Dr César Bergadá (CONICET- Hospital de Niños Ricardo Gutiérrez, Buenos Aires, Argentina). The resulting sequences were analyzed using BLAST and manual alignment. Amino acid sequences corresponding to predicted epitopes were identified from the full-length protein sequences retrieved from BLAST results.

4.2.4. Amino acid sequence, protein structure and physicochemical analysis

The complete amino acid sequences of both GAPDHs were obtained from UniProt. Analysis of differences in GAPDH protein sequences wass carried out using BLAST-P, using the complete sequence of each isoenzyme and a non-redundant database and organism as inputs. Physicochemical properties were analyzed using the ProtParam tool from the Expasy server [64]. Secondary structure prediction of *E. granulosus* GAPDH was conducted using SOPMA [65]. GAPDH domains were predicted using Pfam [66], NCBI [67] and Interpro [68]. Modelling of the tertiary structure was performed using Phyre2 normal mode [69]. The protein models obtained by Phyre2 have been superposed to AlphaFold3 models [70] and the Roo Mean Square Deviation (RMSD) between the two models was evaluated . Model quality was assessed by ProSA-web [71]. To assemble GAPDH monomers into a quaternary structure, we modeled the 222 symmetry homotetramer (biological assembly) using *Leishmania mexicana* GAPDH (PDB code: 1I32) as a template. The model of *Acropora millepora* (PDB code: 6PX2) was used to map the binding sites for substrates Pi, and NAD+.

4.3. Molecular Dynamics Simulation

4.3.1. Native interactions of GAPDH

GAPDH molecular structures were validated through molecular dynamics simulation using the Nanoscale Molecular Dynamics software (NAMD2) [72]. GAPDH was solvated with explicit solvent by using the TIP3 water model. For W6UJ19, the water box size was 114.83 x 122.65 x 107.08 Å (x, y, z), containing 40,077 water molecules. For W6V1T8, the water box was 116.29 x 117.06 x 110.21 Å (x,

 doi:10.20944/preprints202509.1185.v1

y, z), containing 40,085 water molecules. System neutralization was performed to reflect the distinct localization of both enzymes; KCl was used for the IC (W6UJ19) and NaCl for EC isoenzyme (W6V1T8). The ionic concentration was 0.15 mol/L in both cases. All simulations were performed under the periodic boundary conditions. The counterion content was 112 Cl- and 128 K+ atoms and 112 Cl- and 129 Na+, for W6UJ19 and W6V1T8, respectively. All molecular dynamics simulations were performed using the CHARMM36 force field under NPT Ensemble (Isothermal-Isobaric) conditions: constant particle number, pressure (1 atm), and temperature (300 K). The simulation protocols involved 20,000 steps for minimization by the conjugate gradient method plus 144,000 steps (0.288 ns) of heating from 60 to 300K, maintaining the absolute temperature at 300K for the following steps. After, 500,000 steps (1 ns) were performed to equilibration with restrictions in the backbone and finally a 100 ns of unrestrained trajectory was obtained for production. The time of each step was 2 fs. The potential energy throughout the simulation was monitored to confirm the thermodynamic equilibrium of each system. The root mean-square deviation (RMSD) and root mean square fluctuation (RMSF) were calculated. Structures were analyzed and visualized with Visual Molecular Dynamics (version 1.9.3) [73] and Molecular Operating Environment (MOE 2022.20) [74].

- Free energy binding estimation.

The free energy binding between the protein chains and the ligand molecules was estimated by the MMPBSA method using the last 100 frames of each molecular dynamic simulation with the VMD CAFE1.0 tool and the APBS program. For each estimation, the entire molecular system was defined as the complex, the target molecule as the ligand, and all remaining molecules in the system (excluding the ligand) as the receptor.

4.4. Docking and enzymatic dynamic interaction with BP

4.4.1. Docking

The natural substrate of GAPDH, glyceraldehyde-3-phosphate (G3P), Pi and two BP, EHDP (PubChem: CID3305) or AL (PubChem: CID2088) (Figure 13) were docked into the substrate-binding site of each GAPDH enzyme, with NAD+ positioned in its corresponding binding site, using MOE software 2022.20.

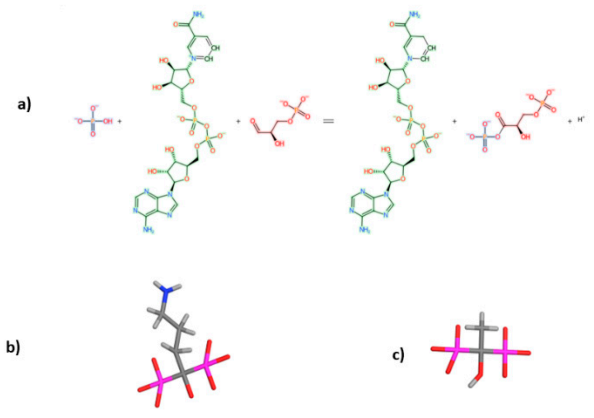

Figure 13. a) Main catalytic reaction of GAPDH showing in green the NAD+ (left) and NADH (right), and the inorganic phosphate and the G3P (left) and 1,3-bisphosphoglycerate (right). b) It shows AL 3D structure and c) it shows EHDP 3D structures.

The Alpha triangle algorithm was used for placement and the London G function for scoring. The Alpha triangle algorithm was selected for ligand placement due to its ability to generate poses by aligning triplets of ligand atoms with triplets of receptor site points. These receptor site points, known as alpha sphere centers, represent regions of tight molecular packing. In each iteration, a

 doi:10.20944/preprints202509.1185.v1

random ligand conformation is selected, and a randomly selected triplet of ligand atoms is aligned with a random triplet of alpha sphere centers to generate a pose. Refinement using the force field, and re-scoring with London G scoring function allowed ranking the top 10 poses. The top scoring pose out of ten poses was selected for further analysis of ligand-protein interactions. Differences among docking scores were analyzed using the student "t" test, considering that each enzyme has 4 subunits, the subunit was considered the single unit analysis.

4.4.2. Molecular Dynamics Interaction

Protein-ligand complexes were prepared for molecular dynamics simulation using MOE software and the QwikMD tool [75] available in VMD 1.9.3, as previously described. A 100 ns production simulation was performed without backbone restraints. Molecular dynamics settings were the same as outlined in section 4.3.1., with modifications in the number of water molecules and ions for each system. For the W6UJ19-EHDP complex, the solvation box contained 40,078 water molecules along with 112 Cl- and 116 K+ ions. For the W6UJ19-AL complex, the system included 40,081 water molecules and 116 Cl-, with 112 K+ ions. In the W6V1T8-EHDP system, 40,084 water molecules were used, along with 112 Cl- and 116 Na+ ions. The W6V1T8-AL system contained 39,980 water molecules and 116 Cl- with 112 Na+ ions. All simulations were executed remotely using NAMD2 on high-performance computing equipment at the Department of Experimentation and Theory of the Structure of Matter and its Applications (DETEMA, Facultad de Química, Universidad de la República, Montevideo, Uruguay). Hardware specifications included: AMD Ryzen 9 5950X processor, RAM 64 GB, RTX 3080 TI GPU, running Ubuntu 22.04.1.

4.5. Searching for Epitopes

4.5.1. Linear Epitopes

Linear epitope prediction was conducted on GAPDH sequences from *E. granulosus*, *T. solium*, *F. hepatica*, *E. multilocularis*, *Bos taurus*, *Ovis aries*, *Homo sapiens*, *and L. mexicana* using eight epitope prediction programs. The B-cell linear epitopes (LEP) for each GAPDH were selected from ABCpred (with a score above 0.85) [76], identified in regions of at least five adjacent amino acids by Bepipred Linear Epitope Prediction 2.0 (threshold: 0.5) or by Bepipred Linear Epitope Prediction (threshold: 0.35), and by at least three of the following software: Chou & Fasman Beta-Turn Prediction (threshold indicated by the server for each protein sequence), Emini Surface Accessibility Prediction (threshold: 1.0), Karplus & Schulz Flexibility Prediction (threshold:1.0), Kolaskar & Tongaonkar Antigenicity (threshold indicated by the server for each protein sequence), and Parker Hydrophilicity Prediction (threshold indicated by the server for each protein sequence) in IEDB (Immune Epitope Database and Analysis Resource)[77]. Post-translational modifications were predicted using MusiteDeep [78] (cut off 0.50) and DeepNitro [79] (cut off medium score).

4.5.2. Conformational Epitopes and Bisphosphonates

B-cell conformational epitopes (Cep) for each GAPDH protein were predicted using DiscoTope 2.0, applying a threshold of -3.7 (sensitivity = 0.47 and specificity = 0.75). Predictions were based on the PDB structures of each GAPDH system at both the beginning and end of the molecular dynamics simulation, including IC and EC isoenzymes under control conditions and after binding with EHDP and AL.

5. Conclusion

We performed the first in silico studies on *E. granulosus* GAPDH, an essential enzyme of the glycolytic pathway involved in host-parasite interactions, recognized by sera from CE patients. Based on predicted linear epitopes in two GAPDH isoenzymes, the IC isoenzyme (W6UJ19) emerged as the

 doi:10.20944/preprints202509.1185.v1

best candidate for the design of multiepitope constructs with potential applications in CE diagnosis and, the ratio between IC and EC isoenzymes must be useful to evaluate treatment success.

Molecular dynamics simulations suggest that the IC isoenzyme has greater enzymatic activity compared to the extracellular (EC) isoenzyme (W6V1T8), supporting its potential as a pharmacological target. Simulations examining the interaction of two BP, EHDP and AL, with both isoenzymes, showed that EHDP (a first-generation BP) exhibits stronger binding affinity than AL. This finding aligns with our previous *in vitro* results using EGPE. Indeed, EHDP due to its limited effect on bone metabolism and its potential antiparasitic effect, EHDP could be a candidate for translational research in infections caused by *E. granulosus* in intermediate hosts. Notably, EHDP shares a structural similarity with PPi, suggesting that endogenous PPi could potentially interact with GAPDH and modulate its enzymatic activity or interfere with EHDP effect but, only PPi is metabolized by endogenous pyrophosphatase. The simulations also provided insights into molecular stability and substrate interactions affected or unaffected by BP binding. Furthermore, we demonstrated how conformational epitopes are altered upon binding of these interactive compounds.

Supplementary Materials: The following supporting information can be downloaded

Figure S1 a , b ,c and d Sequence of glyceraldehyde 3 phosphate dehydrogenase W6UJ19 and W6V!T8 forward and reverse-

Figure S2 Figure Stability of energy in dynamics simulation: Energy in kcal/mol for all GAPDH systems vs time in ns. Green is for electrostatics, red for Van Der Waals and blue for total Potential energy. A: W6UJ19 Control, B: W6UJ19 EHDP, C: W6UJ19 AL, D: W6V1T8 Control, E: W6V1T8 EHDP, F: W6V1T8 AL.

Figure S3 Amino acid interactions in W6UJ19 during molecular dynamics simulation

Figure S4 Amino acid interactions in W6UT1V8 during molecular dynamics simulation

Figure S5 Amino acid interactions in W6UJ19.-EHDP during molecular dynamics simulation

Figure S6 Amino acid interactions in W6UT1V8-EHDP during molecular dynamics simulation

Figure S7 Amino acid interactions in W6UJ19-AL during molecular dynamics simulation

Figure S8 Amino acid interactions in W6UT1V8-AL during molecular dynamics simulation

Table S1 Sires of cofactors and substrate in GAPDH of different species.

Author Contributions: FA performed PCR experiments, in silico and data analysis, and contribute to manuscript writing. AM contributed to in silico data analysis and manuscript writing. MPV performed proteomic protein identification and analysis. AJV contribute with PCR experiments and manuscript writing. EJAR contribute to manuscript writing. MP was a director of in silico experiments and data analysis and contribute to manuscript writing. AGF was research and work director, conceived and designed the results analysis and wrote the manuscript. All authors contributed to the article and approved the submitted version.

Funding: This work was supported by the Fundación Iberoamericana de Estudios Superiores. Chacabuco 90, Buenos Aires, Argentina.

Data Availability Statement: The authors appreciate Miss Claudia Nose for the preparation of the figures, from the National Institute of Parasitology “Dr. Mario Fatala-Chaben,” ANLIS-Malbrán, CABA, Argentina.

Conflicts of Interest: The authors declare no conflicts of interest.

References

1. Vuitton, D. A.; McManus, D. P.; Rogan, M. T.; Romig, T.; Gottstein, B.; Naidich, A.; et al. International consensus on terminology to be used in the field of echinococcoses. *Parasite* **2020**, 27, 41. doi: 10.1051/parasite/2020024
2. Cucher,M. A.; Macchiaroli, N.; Baldi, G.; Camicia, F.; Prada, L.; Maldonado, L.; et al. Cystic echinococcosis in South America: systematic review of species and genotypes of *Echinococcus granulosus* sensu lato in humans and natural domestic hosts. *Trop. Med. Int. Health.* **2016**, 21,166–175. doi: 10.1111/tmi.12647
3. *https://www.who.int/es/news-room/fact-sheets/detail/echinococcosis* (view April 19, 2023)

 doi:10.20944/preprints202509.1185.v1

4. Avila, H. G.; Maglioco, A.; Getiser, M. L.; Ferreyra, M. P.; Ferrari, F.; Klinger, E.; et al. First report of Cystic echinococcosis caused by *Echinococcus granulosus* sensu stricto/G1 in *Felix catus* from the Patagonian region of Argentina. *Parasitol. Res*. **2021**,120, 747–750. doi: 10.1007/s00436-021-07048-
5. Tercero, Gutiérrez, M.J.; Olala, Herbosa, R. Hidatidosis una zoonosis de distribución mundial. *OFFARM*.**2008**, 27, 88-94. https://www.elsevier.es/es-revista-offarm-4-pdf-13127387.
6. Tévez, Craise. L.; Daiana, Vaccaro. R.; De, Luca, P.A.; Vásquez, Guillén, M.E.; Calaramo O.A.; Logioco, F. Hydatidosis: clinical-imaging classification according to Gharbi and the World Health Organization. *Rev. Argent. Radiol*. 2022, 86, 41-48.
7. Tamarozzi, F.; Silva. R.; Fittipaldo, V.A.; Buonfrate. D.; Gottstein, B., Siles, Lucas, M. Serology for the diagnosis of human hepatic cystic echinococcosis and its relation with cyst staging: A systematic review of the literature with meta-analysis. *PLoS Negl. Trop .Dis*. **2021**, 28,15,e0009370. doi: 10.1371/journal.pntd.0009370.
8. Pittini, A.; Martínez, Acosta, Y.E.; Casaravilla, C.; Seoane, P.I.; Rückerl, D.; Quijano, C.; et al. Particles from the *Echinococcus granulosus* laminated layer Inhibit CD40 upregulation in dendritic cells by interfering with Akt activation. *Infect. Immun*. **2019**, 87, e0064,1-19. doi: 10.1128/IAI.00641-19.
9. Barbieri, M.; Fernández, V.; González, G.; Luaces V. M.; Nieto, A. Diagnostic evaluation of a synthetic peptide derived from a novel antigen B subunit as related to other available peptides and native antigens used for serology of cystic hydatidosis. *Parasite Immunol*. **1998**, 20, 51–61. doi: 10.1046/j.1365-3024.1998.00117.x.
10. Sadjjadi, S.F.; Tahereh, Mohammadzadeh, T.; Fatemeh, Hafezi,F.; Sadjjadi ,S.M. Evaluation of the ability of antigen B originated from *Echinococcus granulosus* sensu stricto and *E. Canadensis* for the diagnosis of confirmed human cystic echinococcosis using ELISA. *Iran J. Parasitol*. **2022**, 17,358-465.
11. Echeverría, C. I.; Isolabella, D. M.; Prieto, Gonzalez, E. A.; Leonardelli, A.; Prada, L.; Perrone, A.; et al. Morphological and biological characterization of cell line developed from bovine *Echinococcus granulosus*. *In Vitro Cell. Dev. Biol. Anim*. **2010**, 46, 781–792. doi: 10.1007/s11626-010-9345-8 [
12. Maglioco, A.; Gentile, J.; Barbery, Venturi, M. S.; Jensen, O.; Hernández, C.; Gertiser, M. L.; et al. Detection of *Echinococcus granulosus* sensu lato infection by using extracts derived from a protoscoleces G1 cell line. *Parasite Immunol*. **2019**, 41, e12674. doi: 10.1111/pim.12674
13. Maglioco, M.; Agüero, F.A.; Valacco, M.P.; Juàrez, Valdez, A.; Paulino, M.; Fuchs, A.G. Characterization of the B-Cell Epitopes of *Echinococcus granulosus* histones H4 and H2A recognized by sera from patients with liver cysts. *Front. Cell. Infect. Microbiol.* **2022**, 12, 901994. doi: 10.3389/fcimb.2022.901994.
14. Muronetz, V.I.; Kuravsky, M.L.; Barinova, K.V.; Schmalhausen, E.V. Sperm-specific glyceraldehyde-3-phosphate dehydrogenase - an evolutionary acquisition of mammals. Biochemistry (Mosc), **2015**, 80,1672-1689. doi: 10.1134/S0006297915130040.
15. Ahn, C.S.; Kim, J.G.; Bae, Y.A.; Kim, S.H.; Shin, J.H.; Yang, Y.; et al. Fasciclin-calcareous corpuscle binary complex mediated protein-protein interactions in *Taenia solium* metacestode. *Parasit. Vectors*. **2017**, 10,438. doi: 10.1186/s13071-017-2359-2.
16. Dar, G.H.; Mendes, C.C.; Kuan, W.L. Speciale, A.A.; Conceição, M.; Gorgens, A.;et al. GAPDH controls extracellular vesicle biogenesis and enhances the therapeutic potential of EV mediated siRNA delivery to the brain. *Nat. Commun*. **2021**, 12, 6666. doi: 10.1038/s41467-021-27056-3.
17. Liang, P.; Mao, L.; Zhang, S.; Guo, X.; Liu, G.; Wang, L.; et al. Identification and molecular characterization of exosome-like vesicles derived from the *Taenia asiatica* adult worm. *Acta Trop*. **2019**, 198,105036. doi: 10.1016/j.actatropica.2019.05.027.
18. Quail, E.A.; Yeoh, G.C. The effect of iron status on glyceraldehyde 3-phosphate dehydrogenase expression in rat liver. *FEBS Lett*. **1995**, 359,126-128. doi: 10.1016/0014-5793(95)00023-3.
19. Alvarez, R.A.; Blaylock, M.W.; Baseman, J.B. Surface localized glyceraldehyde-3-phosphate dehydrogenase of *Mycoplasma genitalium* binds mucin. *Mol. Microbiol*. **2003**, 48,1417-1425. doi: 10.1046/j.1365-2958.2003.03518.x.
20. Huang, K.Y.; Huang, P.J:; Ku, F.M.; Lin, R.; Alderete, J.F.; Tang, P. Comparative transcriptomic and proteomic analyze of *Trichomonas vaginalis* following adherence to fibronectin. *Infect. Immun*. **2012**, 8, 3900-3911. Doi:10.1128/IAI.00611-12.

21. Rizvi, S.H.M.; Di, Shao, Tsukahara, Y.; Pimentel, D.R.; Weisbrod, R.M.; Hamburg, M.N.; et al. Oxidized GAPDH transfers S-glutathionylation to a nuclear protein Sirtuin-1 leading to apoptosis. *Free Radic. Biol. Med*. **2021**, 174, 73–83.
22. Lama, A.; Kucknoor, A.; Mundodi, V.; Alderete, J.F. Glyceraldehyde-3-phosphate dehydrogenase is a surface-associated, fibronectin-binding protein of *Trichomonas vaginalis*. *Infect. Immun*. **2009**, 77,2703-11. doi: 10.1128/IAI.00157-09.
23. Sun, S.T.; McKenna, C.E. Farnesyl pyrophosphate synthase modulators: a patent review (2006–2010) *Expert Opin. Ther. Pat*. **2011**, 21,1433–1451. doi: 10.1517/13543776.2011.593511.
24. Docampo, R.; Moreno, S.N.J. Acidocalcisomes. *Cell Calcium*. **2011**, 50,113–119. doi: 10.1016/j.ceca.2011.05.012.
25. Docampo, R.; de, Souza, W.; Miranda, K.; Rohloff, P.; Moreno, S.N.J. Acidocalcisomes—conserved from bacteria to man. *Nat. Rev. Microbiol*. **2005**, 3, 251–261. doi: 10.1038/nrmicro1097.
26. Doggett, J.S.; Schultz, T., Miller, A.J.; Bruzual, I.; Pou, S.; Winter, R.; et al.. Orally bioavailable endochin-like quinolone carbonate ester prodrug reduces *Toxoplasma gondii* brain cysts. *Antimicrob. Agents Chemother*. **2020**, 64,e00535-20. doi: 10.1128/AAC.00535-20.
27. Lai, D.H.; Poropat, E.; Pravia, C.; Landoni, M.; Couto, A.S.; Rojo, F.G.; et al. Solanesyl diphosphate synthase, an enzyme of the ubiquinone synthetic pathway, is required throughout the life cycle of *Trypanosoma brucei*. *Eukaryot. Cell*. **2014**, 13, 320-328. doi: 10.1128/EC.00271-13.
28. Sleda, M.A.; Li, Z.H.; Behera, R.; Baierna, B.; Li, C.; Jumpathong, J.; et al. The heptaprenyl diphosphate synthase (Coq1) is the target of a lipophilic bisphosphonate that protects mice against *Toxoplasma gondii* Infection. *MBio*. **2022**, 13, e0196622. doi: 10.1128/mbio.01966-22.
29. Sleda, M.A.; Pitafi, Z.F.; Song, W.; Oldfield, E.; Moreno, S.N.J. Lipophilic bisphosphonates reduced cyst burden and ameliorated hyperactivity of mice chronically infected with *Toxoplasma gondii*. *MBio*. **2024**, 13,15,e0175624. doi: 10.1128/mbio.01756-24.
30. Valenti, M.T.; Bertoldo, F.; Dalle ,Carbonare, L.; Azzarello, G.; Zenari, S.; Zanatta, M.; et al. The effect of bisphosphonates on gene expression: GAPDH as a housekeeping or a new target gene? *BMC Cancer*. **2006**, 6,49. doi: 10.1186/1471-2407-6-49.
31. Fuchs, A.G.; Echeverría, C.I.; Pérez, Rojo, F.G.; Prieto, González, E.A.; Roldán, E.J. Proline modulates the effect of bisphosphonate on calcium levels and adenosine triphosphate production in cell lines derived from bovine *Echinococcus granulosus* protoscoleces. *J. Helminthol.* **2014**, 88,459-467. doi: 10.1017/S0022149X13000436.
32. Ferrulli, M.; Pérez, Rojo, F. G.; Granada, Herrera, L. A.; Maglioco, A. F.; Roldán, E.A. J.; Fuchs, A.G.. Effect of etidronate and ibandronate on cytosolic Ca2+ in HT29 and parasite cell line from *Echinococcus Granulosus* sensu lato. *The Open Parasitology Journal*. **2019**, 7, 19-25. doi: : 10.2174/1874421401907010019.
33. Ebetino, F.H.; Hogan, A.M., Sun, S., Tsoumpra, M.K.; Duan, X.; Triffitt, J.T.; et al. The relationship between the chemistry and biological activity of the bisphosphonates. *Bone*. **2011**, 49, 20-33. doi: 10.1016/j.bone.2011.03.774.
34. You, J.Q.; Xiao, S.H.; Guo, H.F.; Jiao, P.Y.; Mei, J.Y.; Yao, M.Y.Effect of mebendazole and praziquantel on glucosephosphate isomerase and glyceraldehydephosphate dehydrogenase in *Echinococcus granulosus* cyst wall harbored in mice. *Zhongguo Yao Li Xue Bao*. **1997**, 18, 75-77.
35. Mülle, Schollenberger, V.; Beyer, W.; Schnitzler, P.; Merckelbach, A.; Roth, S.; Kalinna, B.H.; et al. Immunisation with *Salmonella typhimurium*-delivered glyceraldehyde-3-phosphate dehydrogenase protects mice against challenge infection with *Echinococcus multilocularis* eggs. Int. J. Parasitol. **2001**, 31,1441-1449. doi: 10.1016/s0020-7519(01)00244-2.
36. Corbin, I.R.; Gong, Y.; Zhang, M.; Minuk, G.Y. Proliferative and nutritional dependent regulation of glyceraldehyde-3-phosphate dehydrogenase expression in the rat liver. *Cell. Prolif.* **2002,** 35; 173-82. doi: 10.1046/j.1365-2184.2002.00236.x.
37. Herzfeld, J.; Schlesinger, P.A. Analysis of the allosteric basis for positive and negative co-operativity and half-of-the-sites reactivity in yeast and rabbit muscle glyceraldehyde 3-phosphate dehydrogenase. *J. Mol. Biol.* **1975,** 87; 483-517.doi: 10.1016/S0022-2836(75)80055-6.

 doi:10.20944/preprints202509.1185.v1

38. Robbins, A.R.; Ward, R.D.; Oliver, C. A. mutation in glyceraldehyde 3-phosphate dehydrogenase alters endocytosis in CHO cells. *J. Cell. Biol*. **1995,** 130; 1093-1104. doi: 10.1083/jcb.130.5.1093…
39. Iwai, K.; Shibukawa, Y.; Yamazaki, N.; Wada, Y. Transglutaminase 2-dependent deamidation of glyceraldehyde-3-phosphate dehydrogenase promotes trophoblastic cell fusion. *J. Biol. Chem*. **2014,** 289; 4989-4899. doi: 10.1074/jbc.M113.525568.
40. 30. Nakagawa, T.; Hirano, Y.; Inomata, A.; Yokota, S.; Miyachi, K,; Kaneda, M.; et al. Participation of a fusogenic protein, glyceraldehyde-3-phosphate dehydrogenase, in nuclear membrane assembly. *J. Biol. Chem*. **2003,** 278; 20395-20404. doi: 10.1074/jbc.M210824200.
41. Huo, J.; Dong, W.; Xu, J.; Ma, L.; You, C. Role of glyceraldehyde-3-phosphate dehydrogenase (GAPDH) in autophagy activation following subarachnoid hemorrhage. *Exp. Neurol*. **2024,** 371; 114577. doi: 10.1016/j.expneurol.2023.114577.
42. Dan'shina, P.V.; Schmalhausen, E.V.; Arutiunov, D.Y.; Pleten', A.P.; Muronetz, V.I. Acceleration of glycolysis in the presence of the non-phosphorylating and the oxidized phosphorylating glyceraldehyde-3-phosphate dehydrogenases. *Biochemistry (Mosc).* **2003,** 68; 593-600. doi: 10.1023/a:1023968028884.
43. Sundararajj, K.P.; Wood‡, R.E.; Ponnusamy, S.; Salas, A.M.,; Szulc, Z.; Bielawska, A.; et al. Rapid shortening of telomere length in response to ceramide involves the inhibition of telomere binding activity of nuclear glyceraldehyde-3-phosphate dehydrogenase. *J. Biol. Chem*. **2004,** 279; 6152–6162,
44. White, M.R.; Khan, M.M.; Deredge, D.; Ross, C.R.; Quintyn, R.; Zucconi, B.E.; et al. A dimer interface mutation in glyceraldehyde-3-phosphate dehydrogenase regulates its binding to AU-rich RNA. *J. Biol. Chem*.**2015,** 290:1770-1785. doi: 10.1074/jbc.M114.618165.
45. Das, P.; Mukherjee, A.; Adak, S. Glyceraldehyde-3-phosphate dehydrogenase present in extracellular vesicles from *Leishmania major* suppresses host TNF-alpha expression. *J. Biol. Chem*. **2021,** 297; 01198. doi: 10.1016/j.jbc.2021.101198.
46. You, J.Q.; Xiao, S.H.; Guo, H.F.; Jiao, P.Y.; Mei, J.Y.; Yao, M.Y. Effect of mebendazole and praziquantel on glucosephosphate isomerase and glyceraldehydephosphate dehydrogenase in *Echinococcus granulosus* cyst wall harbored in mice. *Zhongguo Yao Li Xue Bao*. **1997,** 18; 75-77.
47. Müller,Schollenberger, V.; Beyer, W.; Schnitzler, P.; Merckelbach, A.; Roth, S.; Kalinna, B.H.; et al. Immunisation with Salmonella typhimurium-delivered glyceraldehyde-3-phosphate dehydrogenase protects mice against challenge infection with *Echinococcus multilocularis* eggs. *Int. J. Parasitol*. **2001,** 31; 1441-149. doi: 10.1016/s0020-7519(01)00244-2.
48. Maglioco, A.; Miana, V.; Valacco, M.P., Agüero, F.A.; Gertiser, M.L.; Avila H.G.; et al., First comparative proteomic and in vitro behavioral study of *Echinococcus granulosus* metacestodes in *Felis catus*. *Fr. Vet. Sc.* **2025,** 12.doi: 10.3389/fvets.2025.1546420.
49. Wang, J.; Li, Y.; Pan, L.; Li, J.; Yu. Y.; Liu, B. et al. Glyceraldehyde-3-phosphate dehydrogenase (GAPDH) moonlights as an adhesin in *Mycoplasma hyorhinis* adhesion to epithelial cells as well as a plasminogen receptor mediating extracellular matrix degradation. *Vet. Res*. **2021,** 52;:80. doi: 10.1186/s13567-021-00952-8.
50. Barbosa, M.S.; Báo, S.N.; Andreotti, P.F.; de, Faria, F.P.; Felipe, M.S.; dos, Santos, Feitosa, L.; et al. Glyceraldehyde-3-phosphate dehydrogenase of *Paracoccidioides brasiliensis* is a cell surface protein involved in fungal adhesion to extracellular matrix proteins and interaction with cells. *Infect. Immun*. **2006,** 74; 382-9. doi: 10.1128/IAI.74.1.382-389.2006.
51. Russell, R.G. Bisphosphonates: mode of action and pharmacology. *Pediatrics* **2007,** 2; S150-S162. doi: 10.1542/peds.2006-2023H.
52. Duff, S.M.; Moorhead, G.B.; Lefebvre, D.D.; Plaxton, W.C. Phosphate starvation inducible ; bypasses' of adenylate and phosphate dependent glycolytic enzymes in *Brassica nigra* suspension cells. *Plant. Physiol.* **1989,** 90; 1275-1278. doi: 10.1104/pp.90.4.1275.
53. Li, Y.K.; Boggaram, J.; Byers, L.D. Alkylation of glyceraldehyde-3-phosphate dehydrogenase with haloacetylphosphonates. An unusual pH-dependence. *Biochem. J.* **1991,** 275; 767-773. doi: 10.1042/bj2750767.
54. Dan'shina, P.V.; Schmalhausen, E.V.; Arutiunov, D.Y.; Pleten', A.P.; Muronetz, V.I. Acceleration of glycolysis in the presence of the non-phosphorylating and the oxidized phosphorylating glyceraldehyde-3-phosphate dehydrogenases. *Biochemistry (Mosc).* **2003,** 68;593-600. doi: 10.1023/a:1023968028884.

55. Felix, R.; Fast, D.K.; Sallis, J.D.; Fleisch, H. Effect of diphosphonates on glycogen content of rabbit ear cartilage cells in culture. *Calcif Tissue Int.* **1980,** 30; 163-166. doi: 10.1007/BF02408621.
56. Felix, R.; Fleisch, H. Effect of diphosphonates on ATP and Pi content, Pi uptake and energy charge of cultured calvaria cells. *Experientia* **1982,** 8; 644-646. doi: 10.1007/BF01964068.
57. Cancela, M.; Paes, J.A.; Moura, H.; Barr, J.R.; Zaha, A.; Ferreira, H.B. Unraveling oxidative stress response in the cestode parasite *Echinococcus granulosus*. *Sci. Rep*. **2019,** 9; 5876. doi: 10.1038/s41598-019-52456-3.
58. Fleisch, H. Bisphosphonates in bone disease: from the laboratory to the patients. **2000** (4th Ed.). *Academic Press*.
59. Russell, R.G.G.; Wats, N.B.; Ebetino, F.H. ; Rogers, M.J. Mechanisms of action of bisphosphonates: similarities and differences and their potential influence on clinical efficacy. *Osteoporos. Int*. **2007,** 19:733-759.doi: 10.1007/s00198-007-0540-8
60. Ye, P.; Yang, Y.; Qu, Y.; Yang, W.; Tan, J.; Zhang, C.; et al. LL-37 and bisphosphonate co-delivery 3D-scaffold with antimicrobial and antiresorptive activities for bone regeneration. *Int. J. Biol. Macromol.* **2024,** 277; 134091. doi: 10.1016/j.ijbiomac.2024.134091.
61. Xia, Y.; Xie, Y.; Yu, Z.; Xiao, H.; Jiang, G.; Zhou, X.; et al. The mevalonate pathway is a druggable target for vaccine adjuvant discovery. *Cell* **2018,** 175; 1059-1073.e21. doi: 10.1016/j.cell.2018.08.070.
62. https://www.uniprot.org/uniprotkb?query=%22Glyceraldehyde%203-phosphate%20dehydrogenase%22%20AND%20(taxonomy_id:6210) (view June 28, 20223)
63. Ye, J.; Coulouris, G.; Zaretskaya, I.; Cutcutache, I.; Rozen, S.; Madden, T.L. Primer-BLAST: a tool to design target-specific primers for polymerase chain reaction. *BMC Bioinformatics*. **2012**, 3,134. doi: 10.1186/1471-2105-13-134.
64. Wilkins, M.R.; Gasteiger, E.; Bairoch, A.; Sanchez, J.C.; Williams, K.L.; Appel, R.D.; et al. Protein identification and analysis tools in the ExPASy server. *Methods Mol. Biol*. **1999,** 12; 531-552. doi: 10.1385/1-59259-584-7:531.
65. Combet, C.; Blanchet, C.; Geourjon, C.; Deléage, G. NPS@: network protein sequence analysis. *Trends Biochem. Sci.* **2000**, 25,147-150. doi: 10.1016/s0968-0004(99)01540-6.
66. Mistry, J.; Chuguransky, S.; Williams, L.; Qureshi, M.; Salazar, G.A.; Sonnhammer, E.L.L.; et al. Pfam: The protein families database in 2021. *Nucleic Acids Res*. **2020**, doi: 10.1093/nar/gkaa913
67. Lu, S.; Wang, J.; Chitsaz, F.; Derbyshire, M.K.; Geer, R.C.; Gonzales, N.R.; et al. CDD/SPARCLE: the conserved domain database in 2020. *Nucleic Acids Res*. **2020.** 48; D265-D268. doi: 10.1093/nar/gkz991.
68. Paysan, Lafosse, T.; Blum, M.; Chuguransky, S.; Grego, T.; Pinto, B.L.; Salazar, G.A.; et al. InterPro in 2022. *Nucleic Acids Res.* **2023**, 51, D418-D427. doi: 10.1093/nar/gkac993.
69. Kelley, L.A.; Mezulis, S.; Yates, C.M.; Wass, M.N.; Sternberg, M.J. The Phyre2 web portal for protein modeling, prediction and analysis. *Nat. Protoc*. **2015**, 10, 845-858. doi: 10.1038/nprot.2015.053.
70. Döpner, P.; Kemnitz, S.; Doerr, M.; Schulig, L. af3cli: Streamlining AlphaFold3 Input Preparation. *J. Chem. Inf. Model*. **2025**, 5,3886-3891. doi: 10.1021/acs.jcim.5c00276.
71. Wiederstein, M. Sippl, M.J. ProSA-web: interactive web service for the recognition of errors in three-dimensional structures of proteins. *Nucleic Acids Res*. **2007,** 35(Web Server issue); W407-10. doi: 10.1093/nar/gkm290.
72. Phillips, J.C,; Hardy, D.J.; Maia, J.D.C.; Stone, J.E.; Ribeiro, J.V.; Bernardi, R.C.; et al. Scalable molecular dynamics on CPU and GPU architectures with NAMD. *J. Chem. Phys*. **2020,** 153; 044130. doi: 10.1063/5.0014475.
73. Humphrey, W.; Dalke, A.; Schulten, K. VMD: visual molecular dynamics. *J. Mol. Graph.* **1996,** 4;33-38, 27-28. doi: 10.1016/0263-7855(96)00018-5..
74. *Molecular Operating Environment (MOE)*, 2020.09 Chemical Computing Group ULC, 1010 Sherbooke St. West, Suite #910, Montreal, QC, Canada, H3A 2R7, **2022**,
75. Ribeiro, J.V.; Bernardi, R.C.; Rudack, T.; Stone, J.E.; Phillips, J.C.; Freddolino, P.L.; et al QwikMD - Integrative Molecular Dynamics Toolkit for Novices and Experts. *Sci .Rep*. **2016,** 6; 26536. doi: 10.1038/srep26536.
76. Saha, S.; Raghava, G.P. Prediction of continuous B-cell epitopes in an antigen using recurrent neural network. *Proteins*. **2006,** 65; 40-8. doi: 10.1002/prot.21078..

 doi:10.20944/preprints202509.1185.v1

77. Vitam, R.; Blazeska, N.; Marrama, D.; IEDB Curation Team Members; Duesing, S.; Bennett, J.; et al. The Immune Epitope Database (IEDB): 2024 update. *Nucleic Acids Res*. **2025**, 53:D436-D443. doi: 10.1093/nar/gkae1092.
78. Wang, D.; Liu, D.; Yuchi, J.; He, F.; Jiang, Y.; Cai, S.; et al. MusiteDeep: a deep-learning based webserver for protein post-translational modification site prediction and visualization. *Nucleic acids Res.* **2020.** 48, W140–W146. https://doi.org/10.1093/nar/gkaa275
79. Xie, Y.; Luo, X.; Li ,Y.; Chen, L,;. Ma, W.; Huang, J.; et al. DeepNitro: Prediction of Protein Nitration and Nitrosylation Sites by Deep Learning. *Genomics Proteomics Bioinf*. **2018,** 16, 294–306. doi: 10.1016/j.gpb.2018.04.007.